Interstellar Mission Design of a Fusion-Powered Spacecraft to Proxima b

Amelie M. Lutz

Thesis submitted to the Faculty of the
Virginia Polytechnic Institute and State University
in partial fulfillment of the requirements for the degree of

Master of Science
in
Aerospace Engineering

Shane D. Ross, Chair
Scott F. England
Riley M. Fitzgerald

May 2, 2025
Blacksburg, Virginia

Keywords: Nuclear Fusion, Proxima b, Mission Design

Interstellar Mission Design of a Fusion-Powered Spacecraft to Proxima b

Amelie M. Lutz

(ABSTRACT)

Recent significant developments in power production using nuclear fusion allows for a realistic discussion of fusion propulsion systems for spacecraft. This study provides a framework for large-scale spacecraft missions to Proxima b. The instrumentation included in the payload was defined based on missions with similar science objectives and flight conditions. A case study was conducted for three propulsion systems: the Fusion Driven Rocket (FDR), an Inertial-Electrostatic Confinement (IEC) fusion system, and an Antimatter Initiated Microfusion (AIM) system. Each propulsion system, originally designed for shorter interstellar distances, was tailored specifically for a Proxima b mission and analyzes its performance for 4 fuels: D-D, D-He^3, D-T, and p-B^{11}. Additionally, the system performance was examined for a fast and slow flyby of Proxima b, and bounded orbit. The analysis indicated a slow flyby and bounded orbit are most ideal for data collection, and can only be supported by the FDR employing D-He^3 with a mission time of 57 years. Future work includes the investigation into the requirements for communication of data back to Earth and the implementation of an autonomous decision-making architecture that guides the spacecraft at extreme distances.

Interstellar Mission Design of a Fusion-Powered Spacecraft to Proxima b

Amelie M. Lutz

(GENERAL AUDIENCE ABSTRACT)

Interstellar missions to Proxima b spark interest due to the likelihood of its existence within the habitable zone of our closest neighbor, Proxima Centauri. The current state of interstellar mission designs to 4.2 light-years (ly) are limited to gram-sized spacecraft employing solar sails, capable of employing one to two sensors. For such extreme distances, a large-scale space probe may be justified to provide an extensive analysis on the habitability of Proxima b. The substantial propulsion requirements required for a large-scale spacecraft inspires the investigation for alternate means of propulsion.

Recent significant developments in power production using nuclear fusion allows for a realistic discussion of fusion propulsion systems for spacecraft. While these devices do not conform with the compactness requirements for space applications, conceptual designs support the possibility of an interstellar probe to 10,000 AU, about 4% of the journey to Proxima b. A case study was conducted for three propulsion systems that use different methods to ignite and sustain fusion conditions. Each propulsion system, originally designed for shorter interstellar distances, was tailored specifically for a Proxima b mission and analyzes its performance for four fuels.

The instrumentation included in the payload was defined based on missions with similar science objectives and flight conditions. The 500 kg payload mass for the 11 instruments and communications system set the scene for the propulsion system analysis. Fusion event probabilities at given temperatures and species properties for the reactants were defined for the four fuels: Deuterium-Deuterium (D-D), Deuterium-Helium-3 (D-He^3), Deuterium-Tritium (D-T), and proton-Boron-11 (p-B^{11}). The performance was determined for three scaled propulsion systems: Fusion Driven Rocket (FDR), Inertial-Electrostatic Confinement (IEC), and Antimatter Induced Microfusion (AIM). Results for the initial analysis assumed a single fast flyby, including a single boost and coast phase, for mission times between 54-119 years. Due to flyby speeds at Proxima b that drastically exceed expectations from the instrumentation, a deceleration phase was deemed necessary.

The single slow flyby scenario, assuming deceleration prior to arrival at Proxima b, and bounded orbit scenario can only be supported by the FDR employing D-He^3 fuel with a mission time of 57 years. Future work includes further investigation into the relay of data back to Earth and the implementation of an autonomous guidance system for interstellar spacecraft. This study demonstrates the possibility for a large-scale spacecraft mission to Proxima b within 60 years.

Dedication

To my family, especially Aldwin Tuazon and Angela Lutz, for your endless encouragement and love throughout this journey.

And to my friends who became family, for the KBBQ, Brecotea, carrying me (temporarily), not letting me get lost in the mountains, and more.

Acknowledgments

First and foremost, I would like to express my sincere gratitude to the National GEM Consortium and Johns Hopkins University Applied Physics Laboratory for the guidance, support, and experiences that I have gained throughout my graduate school journey. Special thanks to my mentors and friends at APL, including Daniel Eby, Sanjiv Shah, Josias Beaubrun, Jordan Kreh, David Wolmark, Brian Loughery, Steven Storck, Isaiah Taylor, Anthony (TJ) Jackson, Miriam Grap, Ann Pollack, Jill Clevenger, and Latonya Robinson.

I want to give my deepest appreciation to Dr. Shane Ross for seeing the potential in this research from the beginning and for his invaluable guidance and support through its completion. In addition, I would like to acknowledge my committee members, Dr. Scott England and Dr. Riley Fitzgerald, for their time, insights, and valuable feedback. I am especially grateful to Dr. Tremayne Waller and Dr. Kaiya Jennings for their sustained guidance, encouragement, and commitment to student success, which have made a lasting impact on my work and on the academic journeys of many others.

Finally, I would like to thank my friends from Virginia Tech for sharing countless breakfastlunchdinners with me, keeping me motivated through the long nights at DDS, and for the positivity and inspiration they bring.

Contents

List of Figures

List of Tables

List of Abbreviations

Subscript Symbols

$_1$	Species 1
$_2$	Species 2
$_F$	Final
$_I$	Initial (mass)
$_L$	Liner
$_0$	Initial
$_a$	Antimatter
$_{br}$	Bremsstrahlung
$_b$	Burning
$_{c.r.}$	Cyclotron Radiation
$_c$	Confinement
$_{ex}$	Exhaust
$_e$	Electrons
$_{fus}$	Fusion
$_i$	Ions
$_j$	Stage number
$_{ne}$	Neutrons
$_{PL}$	Payload
$_P$	Propellant
$_S$	Structural
$_T$	Total

Regular Symbols

α_{CAP}	Specific mass of capacitors (kg/kW)
α_l	Fractional energy lost
α_{SEP}	Specific mass of solar electric panels (kg/kW)
β	Fusion power gain
χ	Stage fraction
ΔV	Change in velocity (cm/s)
$\dot{m}_{ex}$	Exhaust flow rate (g/s)
ϵ	Fraction of fuel mass converted to energy
η_T	Thrust Efficiency Factor
$\eta_{e,i}$	Grid transparency
η_{eff}	Energy utilization efficiency
γ	Fractional power carried by neutrons
γ_{LF}	Lorentz-Fitzerald Contraction Factor
λ	Structure to propellant mass ratio
$\mathcal{M}$	Molar Mass (g/mol)
μ	Reduced mass of colliding particles
ϕ_{ion}	Ionization energy of the lithium liner (74945 kJ/kg)
σ	Cross section (m^2)
a	Acceleration (g)
b	Burnup fraction
C	Fusion Constant (4.3×10^{-8})
c	Speed of light (3×10^{10} cm/s)
$C_{1,2}$	Constants
D	Distance (m)
E	Energy (MeV)

E_{in}	Energy input to the fusion reaction
E_{in}	Input Energy (kJ)
E_k	Kinetic Energy (kJ)
F	Thrust (g-cm/s^2)
f	Frequency of operation (s^{-1})
g_0	Gravity (980 cm/s^2)
G_F	Fusion Gain
G_I	Ignition Gain
I_{sp}	Specific Impulse (s)
k_B	Boltzmann Constant (1.38×10^{-23} cm$^3/s$)
k_H	Hole scaling factor
L	Total distance to destination (cm)
M	Mass (g)
m	Species mass (g)
MR	Mass Ratio
MT	Mission time (years)
n	Particle concentration (particles/cm^3)
N_{cusp}	Number of cusps
N_{R0}	Avogadro's Number (6.022×10^{23} atoms/mol)
n_{st}	Total number of stages
P	Power (MW)
P_{SEP}	Power for solar panels (kW)
Q	Energy released per reaction (eV)
R	Radius (cm)
r_e	Edge radius (cm)

r_{core}	Core radius (cm)
T	Temperature (K)
t	Time (s)
u	Velocity (cm/s)
V_f	Fuel volume (cm^3)
V_L	Liner velocity (m/s)
w	Exhaust velocity (cm/s)
W_F	Final (dry) weight (g-cm/s^2)
x	Fuel species ratio
X_T	Distance traveled (cm)
y	Fuel fraction of species 2
Z	Atomic Number
$<\sigma v>$	Reactivity (cm^3/s)

Superscript Symbols

¯	Average
’	in keV

Chapter 1

Introduction

As science fiction writings have inspired dreams of interstellar travel, the rapid development of technology creates a reality of unmanned missions outside of this solar system. In 2017, NASA created a mission proposal to Alpha Centauri, a triple-star system approximately 4.25 light years (ly) from the Sun[1]. The exoplanet Proxima b sparks a particular interest due to its orbit in the habitable zone of Proxima Centauri[2].

Initial conceptual designs for a mission to Alpha Centauri, such as Breakthrough Starshot, described gram-sized satellites to a significant fraction of the speed of light using solar sails[3]. Assuming that these nanosatellites do not face issues with overheating or collide with dust within the interstellar medium on its round-trip mission, the one to two sensors onboard are limited to experiments that can provide reasonable data at 0.2 c. The solar sail could use the light from Proxima Centauri to slow down near Proxima b and accelerate on its journey back; however, the luminosity of Proxima Centauri is only 0.0015 $L_\odot$ [2].

For a mission of such extreme distances, the inclusion of instruments that collect extensive data on the structure, composition, and activity of Proxima b may be justified to accurately assess its habitability. However, a gap exists in literature for an Alpha Centauri mission using large scale space probes due to the substantial propulsion requirements. Though solar sails provide a reasonable means of propulsion with the current state of technology, the loss of thrust with increasing distance from the sun provides an ineffective means of propulsion for extreme distances[4]. Recent significant developments in power production using nuclear fusion inspire the discussion for using alternate sources of propulsion.

One of the main arguments against using nuclear fusion for propulsion was the realization of igniting and sustaining a fusion reaction such that it produces a high gain[1]. In 2022, Lawrence Livermore National Laboratory was the first to achieve a fusion net gain using a controlled fusion experiment at the National Ignition Facility[5]. The future of fusion for propulsion is now seemingly possible; however, the current state of fusion technology does not support the compactness requirements for space applications. While literature on fusion devices proposed for space propulsion support interstellar probes, the distance for which they are expected to travel does not generally exceed 10,000 AU.

The main contribution of this work is to address the lack of knowledge regarding the realistic application of fusion propulsion to travel extreme interstellar distances for a large-scale space probe. The framework for a fusion-powered spacecraft to Proxima b is created by defining the desired instruments to fulfill mission operations, quantifying the performance of fusion devices using different confinement systems and fuels, and outlining the trajectory requirements that support this mission.

1.1 Proxima b

Proxima b was first identified in 2016 orbiting Proxima Centauri, a red dwarf within the Alpha Centauri star system[6].

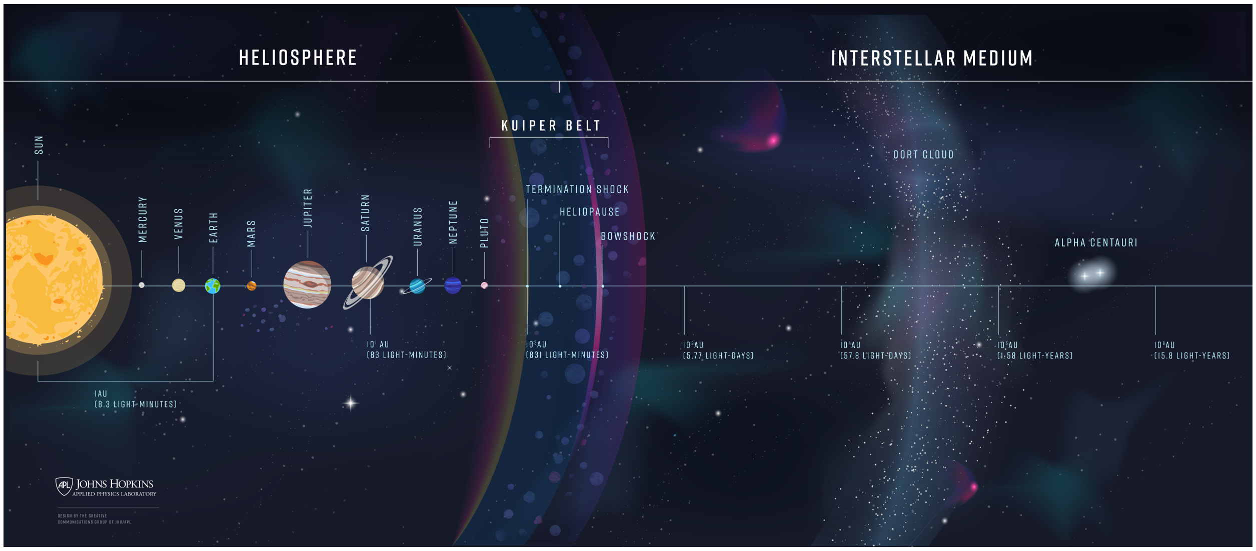

Figure 1.1: Journey to Alpha Centauri (Image Credits: Johns Hopkins APL)[7]

The exoplanet is expected to have sufficient brightness for observational experiments and an atmosphere either close to or thinner than Earth[8]. Proxima b is also subject to at least 30 times more EUV radiation and 250 times more X-rays than Earth[2]. Comparable to the size of Earth, Proxima b has a mass of approximately 1.3 $M_{\oplus}$, orbital period of approximately 11.2 days, and semi-major axis of about 0.05 AU[6]. The properties and relative position of Proxima b with respect to Proxima Centauri suggests an orbital velocity of ~47 km/s.

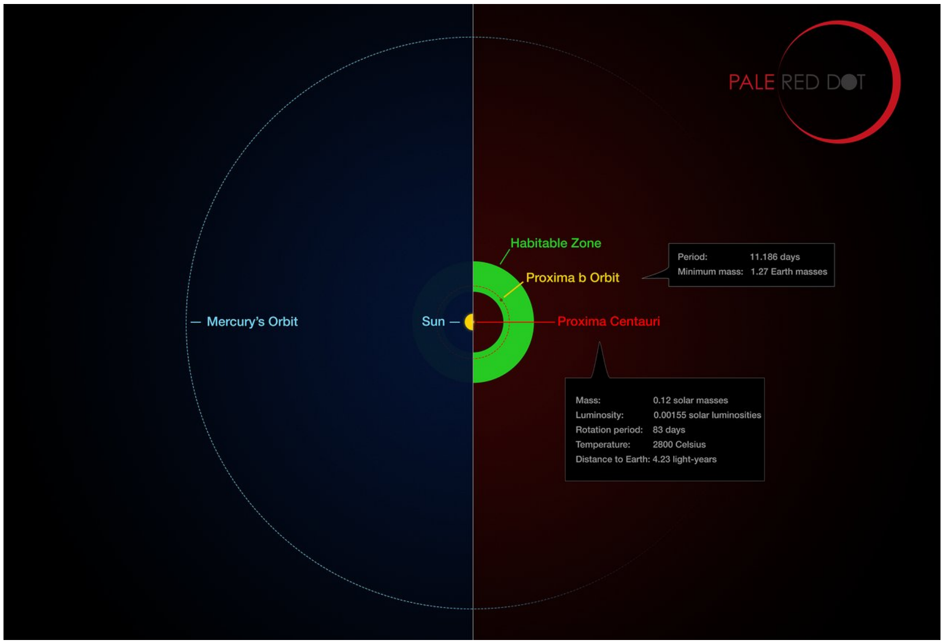

Figure 1.2: Comparable properties of Proxima b (Image Credit: ESO/M. Kornmesser/G. Coleman)[9]

Considering the minimum mass of Proxima b and different scenarios of orbital inclination, the exoplanet has a terrestrial probability of about 84%[10]. Previous analysis on the habitability of Proxima b showed that the proposed CO_2 pressures suggest that liquid water may be present on surface[10]. An investigation on the atmospheric composition, specifically the indication of volatile species and non-condensible gases, will provide valuable insight into the habitability of Proxima b[8]. The properties of Proxima b set the stage for instrumentation and shielding requirements for the spacecraft.

1.2 Background

The current state of fusion research prioritizes finding a method for clean energy production on Earth[11]. Therefore, the most prominent fusion devices, such as tokamaks and stellerators, are very large and unsuitable for use in space. These devices induce and contain fusion conditions using strong magnetic fields, while devices using inertial confinement use a powerful laser to compress fuel into fusion conditions[1].

Confinement methods lower on the technology readiness scale include magneto-inertial fusion (MIF) and inertial electrostatic confinement (IEC). Both systems provide a more compact and powerful alternative to the traditional magnetic and inertial systems, but present significant technical challenges in its current state[1].Antimatter annihilation provides a significantly larger energy output per reaction; however, sourcing of antimatter (specifically antiprotons) is very limited and expensive[12]. Therefore, antimatter annihilation is generally avoided but provides a promising option for inducing fusion conditions, drastically reducing the mass and volume demands of fusion devices[13].

Four fuels were considered: D-D, D-He^3, D-T, and p-B^{11}. The pure deuterium (D-D) reaction is preferred for its simplicity and easy sourcing[14]. Introducing Helium-3 into the mixture (D-He^3) provides an aneutronic product with a high energy output; however, He^3 is very difficult to find in abundance[14]. A deuterium-tritium (D-T) mixture results in a high energy product, is easier to ignite, and is sourced in higher abundance than He^3, but introduces challenges including tritium and neutron management[14]. Lastly, a proton-$Boron^{11}$ (p-B^{11}) fuel uses reactants that are simple to source and has an aneutronic product, but requires a high ignition temperature for a relatively low energy product[15].

A large argument against using fusion fuels in spacecraft is the introduction of radioactive particles, including tritium and free neutrons[15]. This is specifically an issue with D-D and D-T fuels; however, options are in development to address this issue, including the incorporation of radiators, materials for radiation shielding, and breeding blankets surrounding the plasma core[16]. Aneutronic fuels are ultimately preferred for its safety considerations but require higher temperatures from the driver[17].

A property of fusion reactions that characterize the probability of an event occurring is its reactivity. The methods for determining reactivity for the four fuels at different temperatures was discussed and provides a foundation for much of the propulsion system analysis[18].

Three propulsion systems were considered: the Fusion Driven Rocket (FDR), Inertial-Electrostatic Confinement (IEC), and Antimatter Induced Microfusion (AIM). The FDR directly releases energy to produce thrust, resulting in a powerful performance for fuels with high energy products[19] The IEC provides a more compact design but has significant technical challenges, contributing to high loss from the confinement system[20]. Finally, AIM is the most compact and lightweight system, but would only be ideal if a sufficient amount of antiprotons are available[21].

The performance of each propulsion system is compared based on the payload ratio and total mission time. Since the payload consists mainly of instruments which aid the scientific objectives of the mission, a high payload ratio indicates a more cost-effective mission. The total mission time includes the propulsion and coast phases, where a shorter mission time is preferred.

The instruments aboard the space probe face limitations based on the flyby speed, altitude in relation to the surface of Proxima b, and the number of flybys conducted. Much of the instrumentation was in reference to the Europa Clipper and New Horizons missions due to its similarity of scientific objectives and mission profiles[22,23]. For an unregulated propulsion system after the initial burn, the spacecraft will likely pass Proxima b at a speed unacceptable for data collection from the instrumentation. Therefore, the single flyby may require a deceleration phase before approaching its subject of observation. However, instruments that require multiple data sets can only be implemented on a spacecraft intended for multiple flybys. Three mission profiles are considered for their feasibility considering the instrumentation requirements, propulsion system performance, and fuel types.

Chapter 2

Instrumentation

The objective of each instrument selected for the science payload is to provide an analysis of the structure, composition, and activity of Proxima b, used to either support or reject the prospect of habitability. In preparing which instruments should be implemented in the spacecraft, the following assumptions were made

- Technology in its infancy will undergo substantial development before implementation on the spacecraft.
- Instruments receive adequate shielding while inside a radiation vault.

The instrumentation mass and system requirements provided a boundary condition for the overall design of the space probe and, therefore, the propulsion requirements.

2.1 Magnetometer

To characterize the magnetic field of Proxima b, a magnetometer was based on the architecture of the Europa Clipper Magnetometer (ECM). The ECM was originally designed to measure the magnetic field of Europa, requiring a minimum of 12 widely distributed flybys to determine the ice shell thickness, ocean thickness, and ocean salinity with respect to its conductivity[24]. Therefore, the adaptation of this magnetometer assumes a bounded orbit with multiple flybys of Proxima b. Limitations to the approach distance must be 110 km for the magnetometer to provide a reliable induction response. The device is expected to have a mass of 31 kg, a minimum operational power of 16.2 W, and an approximate data volume of 50 Mb/hour.

Considering a single flyby scenario of Proxima b, current magnetometer technologies may not provide accurate measurements of the exoplanet's magnetic field during different environmental conditions. However, the Silicon Carbide Magnetometer (SiCMag) addresses such challenges due to its expected survivability in extreme environments, small-scale, and self-calibration capabilities[25]. The SiCMag, classified as a micro-device, is lightweight and requires minimal power and volume, making it ideal for application on an interstellar space probe. No specific numbers were indicated for SiCMag; therefore, it was assumed that the mass and power requirements were very small compared to the large-scale technology used in the spacecraft. The magnetometer in both trajectory cases would operate between the entry and exit phases of each flyby.

2.2 Magnetic Sounding

Alongside the magnetometer, the magnetic field will be analyzed with respect to the plasma composition to further characterize the habitability of Proxima b. Based on the Plasma Instrument for Magnetic Sounding (PIMS) used for the Europa Clipper mission, the instrument uses two plasma sensors to identify carbon compounds and determine the thickness and salinity of any ice or oceans present on the exoplanet[26]. The device mass is 15.8 kg and operates at a maximum power of 19.8 W with approximately 22.5 Mb/hour data volume. The magnetic sounding instrument operates from a flyby distance of 13,000 km for magnetospheric activity to 100 km for ionospheric activity.

2.3 Thermal Emission Imaging

The thermophysical properties of Proxima b are evaluated using a thermal emission imaging system. The thermal emission imaging system, referred to as THEMIS, builds upon the design and capabilities of THEMIS used for the Mars Odyssey spacecraft to collect thermal infrared images that provide insight into geological formations and activity. A particularly valuable reference for the imaging system is the Europa THEMIS (E-THEMIS), that integrates modifications for increased performance, including optical improvements[27]. The device operates at a mass of 19.1 kg, an approximate data volume of 320 Mb/hour, and a maximum operational power of 42.6 W.

A global-scale analysis of Proxima b would reveal more information on the exoplanet's history and potential for habitability. Considering the previous applications for THEMIS, the device was intended to collect data using multiple images, making it most valuable during the bounded orbit scenario for the Proxima b spacecraft. Limitations for a fast flyby scenario may include optical resolution and decreased input data for the pre-existing analysis model.

Row-skipping methodology, used while the ground velocity is faster than the individual field of view (IFOV), may still allow for valuable data to be collected during a single flyby of Proxima b. The THEMIS would collect calibration data during its approach to Alpha Centauri, prior to the flyby, then operate as intended between the entry and exit phases of each flyby.

2.4 Ultraviolet Imaging

To determine the atmospheric and surface composition, an Ultraviolet Imaging Spectrograph (UVS) will be used. The UVS builds on the foundation of the Europa-UVS[22], JUICE-UVS[28], and Juno-UVS[29] to determine the presence of plumes and examine signs of habitability through the analysis of compounds expressed into space. The instrument operates at a maximum power of 8.5 W, has a mass of 19.6 kg, and a data volume of 0.98 Mb/hour. The device operates between the entry and exit phases of the flyby and is ideally suited for the single flyby and bounded orbit scenarios.

2.5 Gravity and Radio Science

The induced magnetic and gravitational fields, indication of plumes, and the interior structure of Proxima b will be examined using a Gravity and Radio Science (G/RS) device. The G/RS was modeled as a variation of the New Horizons Radio Science Experiment (REX)[30] and the Gravity and Radio Science Instrument used on Europa Clipper[31]. The instrument depends on radiometric tracking to give insight into the geochemical and physical models of the exoplanet, and the evidence of gravity will be determined during the spacecraft's approach to Proxima b. Tidal tracking of the subsurface ocean depends on multiple datasets from the instrument and may be limited to the bounded orbit scenario.

The G/RS has a mass of 0.16 kg, uses a maximum power of 1.6 W, and has an approximate data volume of 74.25 Mb/hour. While the radio science instrument is well suited for a multiple flyby scenario, the instrument may still be valuable for a single flyby to provide preliminary data for Proxima b. The device operates as intended in thin atmospheres, but with increased density may include loss of coherence and multiple atmospheric paths. It is assumed that the device will not face performance limitations since the atmospheric density of Proxima b is similar to Earth.

2.6 Mass Spectrometer

The identification of volatiles and organic compounds are a significant factor in determining the oceanic composition of Proxima b. A mass spectrometer aboard the spacecraft will analyze the exosphere to reveal the geochemical model of the exoplanet. Modeled off the Mass Spectrometer for Planetary Exploration Europa (MASPEX) used on the Europa Clipper, the mass spectrometer samples volatiles to characterize the habitability of Proxima b[32]. The instrument operates at a maximum power of 97 W, with a mass of 61.75 kg, and a data volume of 400 Mb/hour. The device primarily operates during the flyby phase and completes post-processing after the event, making it applicable for each flyby scenario.

2.7 Compositional Mapping

Using spectral sampling, the Imaging Spectrometer (IS) will examine geological processes of Proxima b. The IS was based on the Mapping Imaging Spectrometer for Europa (MISE), designed for the Europa Clipper Mission[33]. The IS determines the surface activity and identifies compounds that support habitability on the exoplanet.

The mapping capabilities of the device depend on the spacecraft range to Proxima b, where the device collects samples from 40,000 km (global-scale), 2,000 km (regional-scale), and 100-25 km (local-scale). The assembly's optical elements with its required electronics operate at a maximum power of 51.7 W, has a mass of 50.4 kg, and expected data volume of 5.9 Gb/flyby. Imaging on the local-scale may prove to be challenging for the single flyby scenarios; however, the device is expected to still provide valuable data for all flight scenarios of the spacecraft.

2.8 Radar Sounding

A radar sounder (RS) aboard the spacecraft will assist with examining the ice and oceans of Proxima b. Based on the Radar for Europa Assessment and Sounding: Ocean to Near-Surface (REASON) used for the Europa Clipper mission, a radar penetrates any existing ice shell to examine Proxima b from the exosphere to its subsurface ocean[34]. Through radar altimetry, reflectometry, sounding, interferometry, plasma characterization, and ranging, a collection of characterizing data will reveal the structure and composition of Proxima b.

The RS has a mass of 105 kg, a maximum operational power of 111 W, and a data volume of approximately 800 Mb/hour. To ensure that all experiments are run under the RS's objectives, the flyby distance must be within 1000 km, with many tasks occurring in the 400-35 km range. Limitations of this device include its intended use for a multiple flyby mission, making it ideal for the bounded orbit scenario; however, valuable data may still be collected for a single flyby mission.

2.9 Dust Sampling

The surface composition and activity will be examined using a mass spectrometer which analyzes dust within the exosphere. The Dust Mass Spectrometer (DMS), based on the SUrface Dust Analyzer (SUDA) used by Europa Clipper, collects ballistic ejecta particles to identify key compounds indicative of habitability and geochemical processes[35]. The DMS has a mass of 14.8 kg, operates at a maximum power of 20.4 W, and has a data volume of approximately 400 Mb/hour. The device operates once entering the exosphere, sampling dust at different altitudes, then completes post-processing of data after the flyby. The DMS does not depend on multiple flybys and will therefore provide valuable data for each flight scenario.

2.10 Imaging System

Imaging Proxima b depends on two camera systems, each with a distinct purpose and resolution. The Narrow-Angle Camera (NAC), based on the Long-Range Reconnaissance Imager (LORRI) used during the New Horizons mission, focuses on high resolution imaging to reveal surface activity and generate topographic models of Proxima b[36]. The NAC operates at a maximum power of 4.6 W, has a mass of 9 kg, and a data volume of approximately 600 Mb/hour.

The Wide-Angle Camera (WAC), based on the Mercury Dual Imaging System (MDIS) used during the MESSENGER mission, focuses on the surface properties and global-scale mapping of Proxima b[37]. The WAC operates with a maximum power of 19.9 W, has a mass of 9.3 kg, and a data volume of approximately 320 Mb/hour. The camera system begins imaging from a distance of 12,500 km until its closest approach, utilizing an exposure on the millisecond scale between 0 and 30 s, depending on the scope of investigation.

2.11 Communications

A main concern for a one-way spacecraft to Proxima b includes the communication of data from extreme distances while reducing mass, volume, and power requirements. Conceptual interstellar probes make the assumption that communication will be possible using a parabolic antenna at 10,000 AU with a data rate of 100 b/sec using less than 1 kW of power[21]. However, simply scaling this technology for a mission to Proxima b is not feasible. An option for relaying data from the space probe is by taking advantage of the solar gravitational lens.

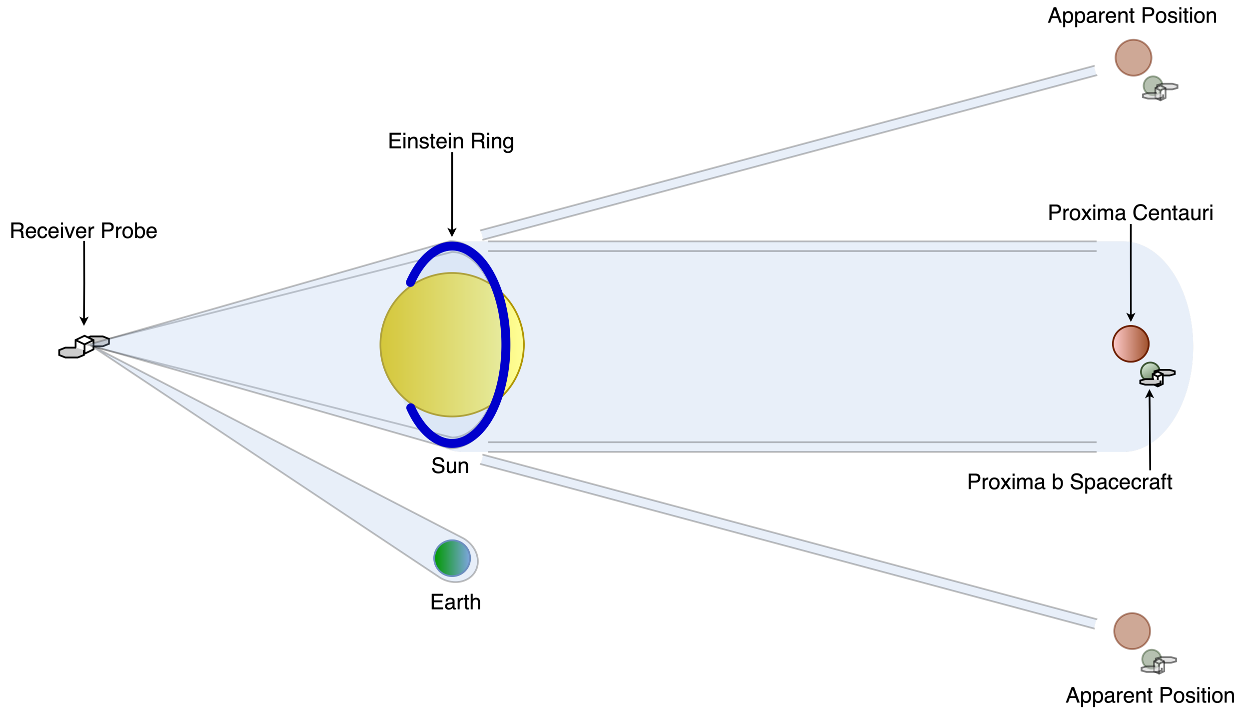

Figure 2.1: 2D representation of the solar gravitational lens communication system.

Using the alignment of a receiver probe with two stars, the gravitational field of the source star (our Sun) allows for the perceived star (Alpha Centauri) to be magnified, where light rays bend around the source star in an Einstein Ring[38].

The spacecraft can emit a laser pulse from a region within the Alpha Centauri system to our Solar System, where another probe within the lens receives the amplified signal at a proposed rate of 10 Mb per second per Watt[38]. The power requirements from the space probe in the Alpha Centauri system will then be drastically reduced; however, the spacecraft will need to be within the lensing region of Alpha Centauri. For this study, the assumption was made that the spacecraft is able to use the solar gravitational lens to communicate data from Alpha Centauri to a receiver probe.

2.12 Instrument Summary

For all instruments discussed, the mass, power, and data volume requirements are compiled in Table 2.1.

Table 2.1: Relevant Specifications for Each Instrument

Instrument Name	Mass (kg)	Operational Power (W)	Data Volume (Mb/hour)
SiCMag *(SF)*	0.1	1	1
Magnetometer *(BO)*	31	16.2	50
Magnetic Sounder	15.8	19.8	22.5
THEMIS	19.1	42.6	320
UVS	19.6	8.5	0.98
G/RS	0.16	1.6	74.25
Mass Spectrometer	61.75	97	400
IS	50.4	51.7	11800
RS	105	111	800
DMS	14.8	20.4	400
NAC	9	4.6	600
WAC	9.3	19.9	320

The science payload specifications differ for the single flyby *(SF)* and bounded orbit *(BO)* scenarios due to the magnetometer requirements from Section 2.1, and are summarized in Table 2.2.

Table 2.2: Instrumentation Data Summary

	Science Payload Mass (kg)	Science Payload Power (W)	Data Volume (Mb/hour)
Single Flyby Scenario	305.01	378.10	14738.73
Bounded Orbit Scenario	335.91	393.3	14787.73

Due to the high collection of data onboard the spacecraft, a machine learning algorithm may be useful to filter out useful data and reduce the data volume from the spacecraft. Additional considerations for the mass and power requirements include, but are not limited to, additional radiators and radiation shielding for the spacecraft and its components. The payload mass to be used for future analyses is rounded up to 500 kg, and the payload power requirements can be rounded up to 1200 W.

Chapter 3

Propulsion System

The propulsion system has a range of configurations to be considered and is evaluated based on two key parameters: the payload ratio and mission time. The fusion environment defines the type of confinement the fuel will be subject to, including how the reaction will be created and sustained. Four types of fusion fuels are considered with advantages to each; however, the efficiency of the energy conversion system ultimately drives the decision towards fuels with higher energy products.

3.1 Fusion Environments

There are four main types of fusion environments that are used to drive and contain fusion events. Though magnetic and inertial confinement methods are more researched and are higher on the technology readiness scale, hybrid systems provide better performance while maintaining a low mass and volume. Antimatter annihilation provides a powerful source of propulsion; however, its limited availability restricts the consideration of this method for propulsion over extreme distances. Instead, antimatter annihilation is proposed as a driver for fusion reactions.

3.1.1 Magnetic Confinement

Magnetic confinement fusion (MCF) describes a plasma subject to strong magnetic fields for containment and to maintain fusion conditions. A number of configurations exist for MCF devices, including tokamaks, stellarators, magnetic mirrors, and spheromaks. MCF devices are ideal for low-density plasmas that need to be sustained for a long time. A significant disadvantage of MCF devices are its high mass and volume demands, which may not be ideal for applications in spacecraft. However, one major advantage of MCF devices is that they are the most developed concept due to the lack of compactness requirements for power production on Earth.

3.1.2 Inertial Confinement

Inertial confinement fusion (ICF) uses a powerful laser to compress and rapidly heat fuel to fusion conditions. This short burst of energy allows for fusion of high ignition temperature fuels, such as p-B^{11}, to be realized. Issues with ICF devices include high precision requirements for the laser with poor system compactness, making it difficult to implement on a spacecraft.

3.1.3 Magneto-Inertial Fusion

Magneto-Inertial Fusion (MIF) acts as a hybrid between MCF and ICF systems, using a pre-magnetized fuel and compressing it rapidly. MIF devices tend to be smaller than its competitors by relieving the powerful driver requirements and reducing the scale of plasma confinement. Due to the precision of the compression and magnetization processes, MIF devices are still very early in its development phase.

3.1.4 Inertial Electrostatic Confinement

Inertial Electrostatic Confinement (IEC) devices confine plasma using an electrostatic potential well, accelerating ions within the fuel into fusion conditions. IEC devices are expected to be compact and lightweight, but may be subjected to major output losses from the selected plasma confinement method. However, if the scientific challenges of IEC systems were to be resolved, the device would theoretically be the most advantageous for its high power output and system compactness.

3.1.5 Antimatter Annihilation

The collision between matter and antimatter results in an energy production significantly larger than fusion and fission reactions. The use of antiproton annihilation to drive a propulsion system can result in a very high specific impulse with little appreciable mass. Each annihilation produces an energy output on the GeV scale, resulting in the highest energy density, and thus a high payload capacity.

$$\mathrm{p} + \bar{\mathrm{p}} \rightarrow \gamma + \gamma + \sim 1.9\ \mathrm{GeV} \tag{3.1}$$

The major limitations of antimatter annihilation are the large quantities of antimatter needed for this system paired with the high cost of production. Antiparticles are not naturally produced on Earth but can be created by particle accelerators, such as with the CERN Low Energy Antiproton Ring[39]. Cosmic ray antiprotons were observed with PAMELA[40] in a belt around Earth; however, extraction from the upper atmosphere may be extremely difficult. Additionally, the storage of antiprotons is possible in Penning Traps for slightly more than 1 year, which does not exceed the requirements for an interstellar mission of this scale.

Instead of a large driver system to produce fusion conditions, antimatter annihilation provides a compact yet powerful alternative to the standard fusion devices described previously. These hybrid systems include the Antiproton-Catalyzed Microfission/fusion (ACMF), Ion Compressed Antimatter Nuclear II (ICAN-II), and Antiproton Initiated Microfission/fusion (AIM). Considering that the main limiting factor of antimatter systems is antiproton sourcing, the AIM device will be investigated due to its relatively lower antimatter usage.

3.2 Types of Fusion Reactions

Four main fuels were considered for the propulsion system that include a combination of the following light nuclei: Deuterium (D), Helium (He), Tritium (T), proton (p), and Boron (B).

$$(50\,\%)\,\mathrm{D} + \mathrm{D} \longrightarrow \mathrm{He}^3\,(0.82\,\mathrm{MeV}) + n\,(2.45\,\mathrm{MeV}) \tag{3.2}$$

$$(50\,\%)\,\mathrm{D} + \mathrm{D} \longrightarrow \mathrm{T}\,(4.04\,\mathrm{MeV}) + p\,(14.67\,\mathrm{MeV}) \tag{3.3}$$

$$\mathrm{D} + \mathrm{T} \longrightarrow \mathrm{He}^4\,(3.52\,\mathrm{MeV}) + n\,(14.06\,\mathrm{MeV}) \tag{3.4}$$

$$\mathrm{D} + \mathrm{He}^3 \longrightarrow \mathrm{He}^4\,(3.67\,\mathrm{MeV}) + p\,(14.67\,\mathrm{MeV}) \tag{3.5}$$

$$\mathrm{p} + \mathrm{B}^{11} \longrightarrow 3\,\mathrm{He}^4\,(8.68\,\mathrm{MeV}) \tag{3.6}$$

Characteristics for each fuel that will be useful for the propulsion system analysis are referenced in Table 3.1.

Table 3.1: Species characteristics.

Species	Molar Mass, $\mathcal{M}$ (g/mol)	Atomic Number, Z
proton (p)	1.0078250	1
neutron (n)	1.0086649	0
Deuterium (D)	2.0141018	1
Helium-3 (He^3)	3.0160293	2
Tritium (T)	3.0160493	1
Helium-4 (He^4)	4.0026033	2
Boron-11 (B^{11})	11.0093052	5

Each reaction has its own advantages; however, aneutronic fuels are usually preferred for applications to spacecraft propulsion due to its simplicity of post-processing.

3.2.1 Reactivity

The probability of a fusion reaction occurring depends on the collision cross section (σ) and relative velocity (v) of the two reactant species. Cross sections for the reactions referenced in this paper were defined for a Maxwellian distribution of incident energies by the Evaluated Nuclear Data File (ENDF) database[41].

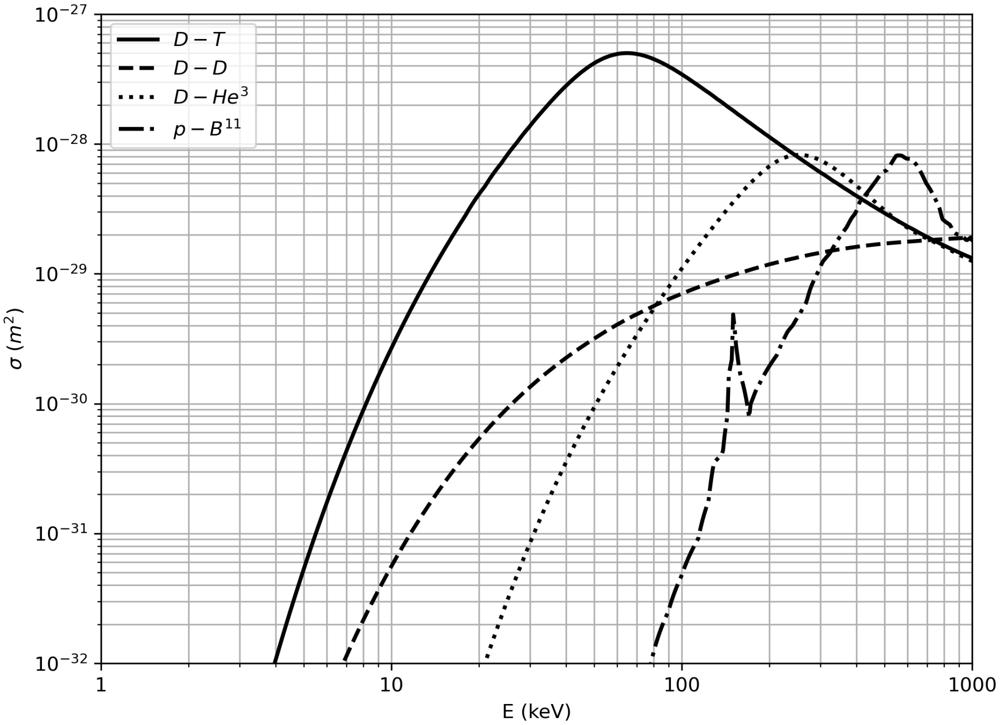

Figure 3.1: Collision cross sections for a Maxwellian distribution of incident energies.

It is important to note that the p-B^{11} first characteristic peak in cross section around 150 keV results from a nuclear resonance with an excited state of C^{12}.

The averaged reactivity ($<\sigma v>$), or reaction rate per unit volume, can then be written for a range of temperatures. To solve the reaction as a one-body problem, the reduced mass of the two species is written as $\mu = m_1 m_2/(m_1 + m_2)$.

$$<\sigma v> = \frac{4}{(k_B T')^{3/2}\sqrt{2\pi\mu}} \int_0^\infty \sigma(E') E' \exp\left(-\frac{E'}{k_B T'}\right) dE' \tag{3.7}$$

The cross section as a function of energy (Figure 3.1) and reactivity as a function of temperature (Table 3.2) were plotted using the code in Appendix A, adapted from Hill[18].

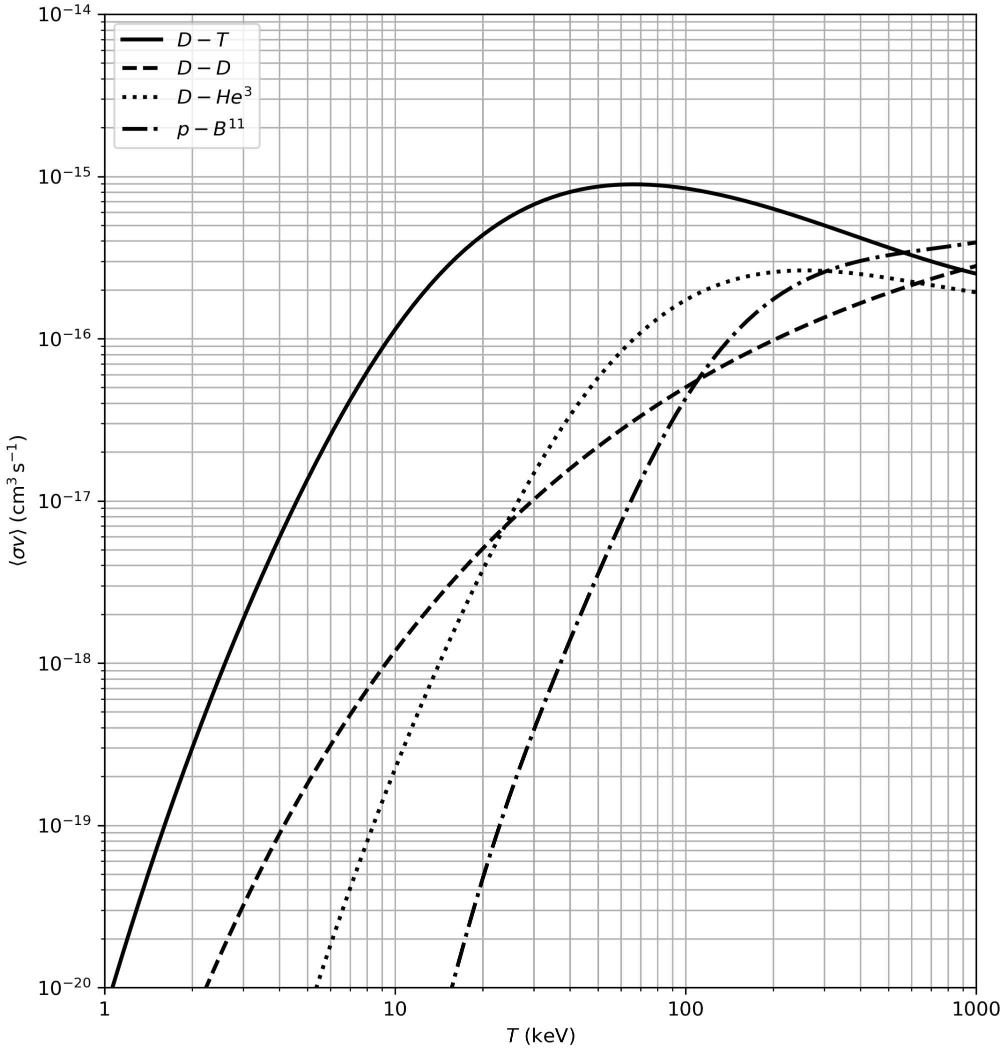

Figure 3.2: Averaged reactivity for a distribution of temperatures.

As demonstrated in the plots, D-T has a peak reactivity near lower temperatures while D-He^3 has a lower peak at a higher temperature. Therefore, while D-He^3 has a higher energy output by definition, more energy will be extracted from a D-T fuel. D-He^3 and p-B^{11} peak at higher temperatures and will require a more powerful driver in order for a fusion event to occur.

3.2.2 Reaction Product Management

The proton-branch of the D-D reaction produces a considerable amount of tritium, which traditionally requires special processing for its radiation properties. In an unmanned spacecraft, radiation shielding remains a requirement for the instrumentation to maintain the integrity of data and the safety of components. Additionally, the tritium product may lead to secondary D-T reactions, producing more neutrons than intended.

Free neutrons produced from fusion reactions may similarly lead to radiation damage and compromise the structural integrity of components. Collisions between free neutrons and external surfaces will contribute to heating of the spacecraft due to a non-negligible transfer of energy from the neutrons. Therefore, fusion devices using D-D or D-T will require a large radiator and a considerable amount of radiation shielding, also adding mass to the spacecraft. Aneutronic fuels, which have a neutron product with less than 1% of a reaction's total energy, are preferred for space applications due to its clean energy properties[15]. Though aneutronic fuels are more difficult to ignite and sustain, its simplicity and compactness make it advantageous for space.

3.2.3 D-D

The D-D reaction results in an approximately 50% yield of either He^3 or T products as demonstrated by Equations 3.2 and 3.3. The products of the D-D reactions may lead to secondary reactions between D-He^3 or D-T; however, only the primary reaction and its energy output are considered during the propulsion system analysis. While the energy output for the reaction appears higher than its competitors, the probability of each reaction results in an averaged 11 MeV energy output for a D-D fuel.

In addition with its high abundance, due to its natural sourcing in the oceans and fresh water[42], D-D reactions are advantageous for its simplicity and accessibility. Additionally, due to a notably lower neutron product than D-T, the reduced cost of product handling is favorable. Compared to other fuels, the D-D reactivity tends to be notably lower, resulting in the tough decision between sacrificing compactness for a more powerful driver or settling for a low energy output.

3.2.4 D-He^3

The use of D-He^3 fuels is a popular choice due to its aneutronic nature and high energy output per fusion event. The lack of radioactive products reduces the radiation shielding and radiator requirements for the spacecraft.

Concerns for D-He^3 fuels include its high temperature requirements to drive fusion conditions and its limited supply on Earth. Sourcing of He^3 comes from tritium processing in CANDU reactors, but can also be found in natural gases and the upper atmosphere[43]. A large amount of the isotope can be found on the lunar surface, and prospects for lunar mining may relieve concerns of He^3 scarcity. Simply reducing the concentration of He^3 to account for a limited supply would result in a higher probability of D-D reactions occurring, therefore compromise the aneutronic properties of the D-He^3 fuel.

3.2.5 D-T

An advantage of D-T fuels is its high energy output and peak reactivity at a reasonable temperature (Figure 3.2). Reactions between D and T have a high neutron product that may contribute to radiation damage and indirect heating of the spacecraft. In addition to radiation shielding, a large radiator or neutron absorber would be required, which significantly increases the structural mass and manufacturing cost.

Tritium is not sourced naturally in large abundance but can be found in nuclear power and government weapons production plants[44]. Proper storage and maintenance of tritium is required to prevent it from decaying, which makes it difficult to handle in space. Fusion devices in development, such as the ITER, use a lithium breeding blanket to produce tritium, which is then extracted and redistributed into the plasma core[45].

$$\mathrm{Li}^6 + \mathrm{n} \longrightarrow \mathrm{T} + \mathrm{He}^4 + (4.8\,\mathrm{MeV}) \tag{3.8}$$

$$\mathrm{Li}^7 + \mathrm{n} \longrightarrow \mathrm{T} + \mathrm{He}^4 + \mathrm{n} - (2.8\,\mathrm{MeV}) \tag{3.9}$$

While Equation 3.8 is the main driver of the tritium breeding, Li^6 is difficult to obtain naturally and likely will come from lithium enrichment. Though the Li^6 within the blanket acts as the primary reaction, the contribution of Li^7 reduces the total recoverable heat from the blanket due to its endothermic nature. Devices that use a breeding blanket relieve the significant tritium management requirements since it no longer needs to maintain a large source of tritium for regular insertion.

While a breeding blanket would be ideal to manage the neutron product from the D-T reactions and develop a self-sustaining tritium source, it may pose an incredible engineering challenge to reduce the scale of the fusion core for spacecraft applications. Recent developments for breeder designs using tungsten alloys for structure and radiation shielding have supported the future of fusion devices in confined spaces[16]. In this case, using D-T as a fuel would be advantageous to provide a high energy output while reducing the concern for radiation shielding and neutron moderation.

3.2.6 p-B^{11}

Similar to D-He^3 fuels, p-B^{11} is a completely aneutronic process whose products decay into three He^3 particles. Boron has two stable isotopes, 80% of which naturally occurs as B^{11} [46]. Boron in nature is mostly extracted from borate compounds that can commonly be found in seawater and various ground sources; therefore, Boron is considered abundant.

The advantages of its aneutronic nature and simple sourcing may not outweigh the high driver requirements and low energy output of a p-B^{11} fuel. The temperature required to ignite and maintain the fusion reaction can be as much as 30 times higher than its competitors, which may be very difficult to achieve[47].

3.3 Fusion Driven Rocket

The Fusion Driven Rocket (FDR) directly releases energy produced by the fusion core into the propellant system[19]. In this section, methods from Slough[19] were applied to the 4 fusion fuels in Section 3.2. Originally proposed for a 90 day manned mission to Mars, the rocket was expected to have a very high specific impulse while using less propellant than other propulsion systems. The FDR uses a type of MIF by employing a magnetized plasmoid and compressing it using metal liners, as demonstrated in Figure 3.3. A compact toroidal plasmoid is injected into a thrust chamber of field-reversed configuration (FRC), where the magnetic field of the plasma core is in the opposite direction of the external magnetic field[48]. The plasmoid is confined by shell driver coils until it is compressed into fusion conditions by converging shell segments. The shell absorbs the plasma energy and becomes ionized before expanding out of the magnetic nozzle, producing thrust without using a large driver.

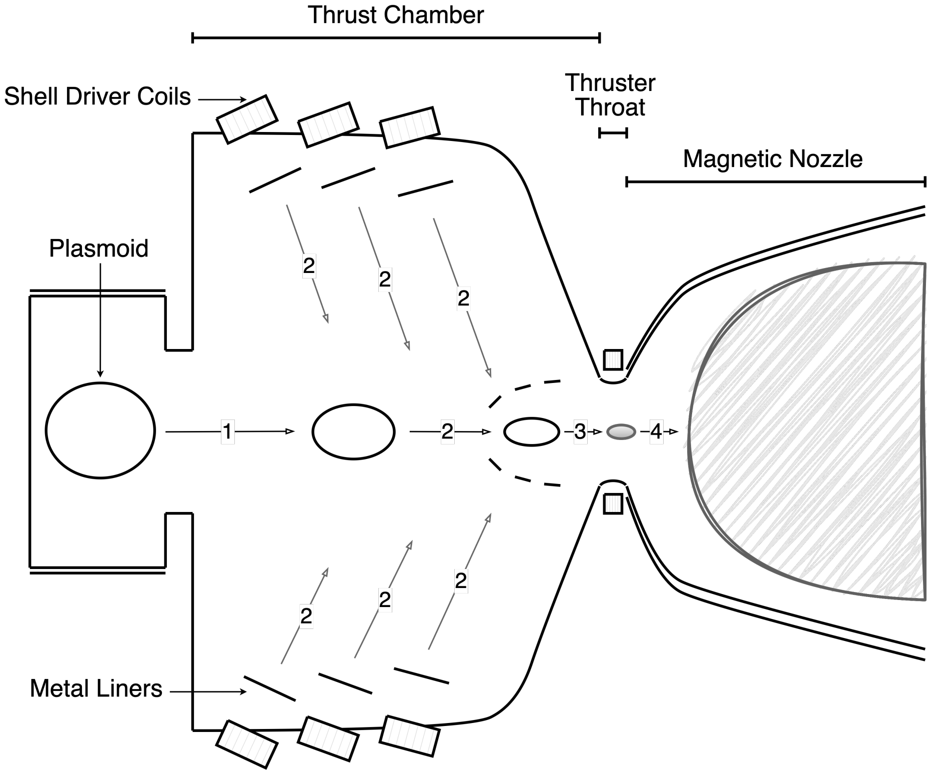

Figure 3.3: FDR thrust production by 1. injection of a plasmoid into the thrust chamber 2. plasmoid confinement in the thrust chamber and compression by metal liners 3. compression into fusion conditions through the thruster throat 4. plasma exit through the diverging nozzle.

To model the FDR for a Proxima b length mission, the upwards scaled lithium liner properties were defined. The liner mass (M_L, in kg) was determined from the minimum mass required to withstand the fusion reaction within the liner. The terminal velocity at which the liner converges (V_L) was set low enough to ensure that it does not match the velocity at which lithium vaporizes. The energy input into the fusion reaction (E_{in}) defines the energy from the liner used to ignite the reaction.

$$E_{in} = \frac{1}{2} M_L V_L^2 \tag{3.10}$$

The ignition gain (G_I) from additional heating of the fusion products was assumed to be at the upper limit of 10. From the ignition gain and energy input, the fusion gain (G_F) could be determined.

$$G_F = M_L^{1/2} G_I C E_{in}^{11/8} \tag{3.11}$$

The kinetic energy (E_k) of the reaction was defined by the output energy of the fusion reaction and includes the energy loss by ionization energy from the liner.

$$E_k = \eta_T G_F E_{in} \ - \ \phi_{ion} M_L \tag{3.12}$$

The projected specific impulse (I_{sp}) was then determined from the kinetic energy of the liner, where the ionization energy loss takes a more significant toll on the specific impulse at lower energies.

$$I_{sp} = \frac{1}{g_0(\frac{m}{s^2})} \sqrt{\frac{2E_k}{M_L}} \tag{3.13}$$

From the rocket equation, the mass ratio ($MR = M_I/M_F$) was calculated using the desired ΔV as a boundary condition.

$$MR = \exp\left(\frac{\Delta V}{I_{sp} g_0}\right) \tag{3.14}$$

Table 3.2 summarizes the inputs and calculated results to define the FDR.

Table 3.2: FDR Design Parameters

M_L (kg)	1.57
V_L (km/s)	17.24
E_{in} (kJ)	233783
G_F	173369
E_k (kJ)	40530977849
$I_{sp}(s)$	731737
ΔV (c)	0.055
MR	9.944
α_{CAP} (kg/kW)	1
α_{SEP} (kg/kW)	0.006
M_{PL} (kg)	500

Solar panels are used to charge the fusion capacitors, which assist with establishing the FRC in the liner. Specific masses for the solar panel and capacitors were defined to meet power demand of the rocket.

$$MR = \frac{M_I}{M_F} \tag{3.15}$$

$$M_F = M_{PL} + M_S \tag{3.16}$$

$$M_I = M_{PL} + M_S + M_P \tag{3.17}$$

$$M_P = M_L f \Delta t \tag{3.18}$$

$$M_S = \frac{E_{in}}{\alpha_{CAP}} + \frac{P_{SEP}}{\alpha_{SEP}} + 0.1 M_{PL} \tag{3.19}$$

$$E_{in} = \frac{P_{SEP}}{f} \tag{3.20}$$

The system of equations provided resultant masses (in kg) and power requirements for the spacecraft.

Table 3.3: Spacecraft mass properties and requirements

M_I (kg)	2707376
M_F (kg)	272257
M_S (kg)	271757
M_P (kg)	2435119
f (s^{-1})	0.00098
P_{SEP} (kW)	229.5

Using the spacecraft properties from Tables 3.2 and 3.3, the FDR performance was determined using methods from Spencer[49]. The input parameters for each fuel were defined, with reactivity from the model used in Section 3.2.1.

Table 3.4: Fuel properties

	D-D	D-He^3	D-T	p-B^{11}
T' (keV)	100	70	20	300
$< \sigma v >_{1,2}$(10^{-16} cm^3/s)	0.5007	1.087	4.341	2.576
$< \sigma v >_{1,1}$ (10^{-16} cm^3/s)	0.01184	0.01184	0.01184	3.361
n_0 (10^{18} cm^{-3})	10	5	5	5
y	0.5	0.5	0.5	0.167
ϵ	0.00097	0.00393	0.00377	0.00078

Using a burnup fraction less than 0.2 and specifications from each fuel, the confinement time (t_c) for the average fuel ion was determined.

$$t_c = \frac{(n_1\mathcal{M}_1 + n_2\mathcal{M}_2)b}{(\mathcal{M}_1 + \mathcal{M}_2)n_1 n_2 < \sigma v >_{1,2} (1 - b\epsilon)} \tag{3.21}$$

The exhaust flow rate ($\dot{m}_{ex}$) is a function of the fuel volume (V_f) and is controlled by the reactivity of the fuel.

$$\dot{m}_{ex} = (n_1\mathcal{M}_1 + n_2\mathcal{M}_2)\,\frac{V_f}{t_c N_{R0}} \tag{3.22}$$

The exhaust velocity relies on the burnup fraction and is highly dependent on the fraction of fuel mass converted to energy.

$$w = c(\epsilon b(2 - \epsilon b))^{1/2} \tag{3.23}$$

From the exhaust flow rate and exhaust velocity, the thrust may be calculated.

$$F = \dot{m}_{ex} w \tag{3.24}$$

To define the power needed from the exhaust (P_{ex}), the thrust and exhaust velocity are used.

$$P_{ex} = (5 \times 10^{-14})Fw \tag{3.25}$$

The fractional power carried by neutrons (γ) and the fractional energy lost ($\alpha_l = \alpha_{l,br} + \alpha_{l,c.r.}$) indicate portions of the total power output that contribute to reduced efficiency.

$$\gamma = \frac{0.5(1-y)^2 < \sigma v >_{1,1} E_{ne}}{y(1-y) < \sigma v >_{1,2} E_{1,2} + 0.5(1-y)^2 < \sigma v >_{1,1} E_{1,1}} \tag{3.26}$$

The bremsstrahlung contribution to energy loss ($\alpha_{l,br}$) is a function of the fuel particle properties and reactivity[50].

$$\alpha_{l,br} = \frac{5.35 \times 10^{-31} n_e (n_1 Z_1^2 + n_2 Z_2^2)(T_e')^{1/2}}{2.93 \times 10^{-12} n_1 n_2 < \sigma v >_{1,2}} \tag{3.27}$$

The fractional power lost by cyclotron ($\alpha_{l,c.r.}$) radiation was reduced due to the assumption of self-absorption in the plasma[51].

$$\alpha_{l,c.r.} = \frac{8.5 \times 10^{-23}[(y+1)\ T_i'\ T_e' + (y+1)^2 (T_e')^2][1 + \frac{T_e'}{204}]}{y(1-y) < \sigma v >_{1,2}} \tag{3.28}$$

The total power output from the device is then defined by

$$P_T = \frac{P_{ex}}{1 - (\gamma + \alpha_l)} \tag{3.29}$$

For each stage (j), burning time for the propellant is calculated using the specific impulse, stage fraction (χ_j), and initial acceleration ($a_{0,j}$). Since a single-stage is assumed, the the stage fraction is 1.

$$t_{b,j} = \frac{(1 - \epsilon b) I_{sp,j}}{(1 + \chi_j) a_{0,j}} \tag{3.30}$$

For the final stage, the burnout velocity is defined by

$$u_{n_{st}} = c \frac{MR^{2 n_{st} w/c} - 1}{MR^{2 n_{st} w/c} + 1} \tag{3.31}$$

The total distance covered for the burning time is

$$X_T \cong \sum_{j=1}^{n} u_{j-1} t_{b,j} + \frac{c^2}{\bar{a}_j g_0} \left[\left(1 + \frac{\bar{a}_j^2 g_0^2 t_{b,j}^2}{c^2} \right)^{1/2} - 1 \right] \tag{3.32}$$

Where the u_{j-1} is the velocity of the previous stage, and the average acceleration (in g) per stage is

$$\bar{a}_j = \frac{a_{0,j}}{2} \left(\frac{2\chi_j + 1}{\chi_j} \right) \tag{3.33}$$

Then the total time to a distance of L is

$$MT = 3.18 \times 10^{-8} \left[n_{st} t_{b,j} + \frac{L - X_T}{u_{n_{st}}} \right] \tag{3.34}$$

Results from the FDR performance analysis is represented in Table 3.5.

Table 3.5: FDR performance analysis results

	D-D	D-He^3	D-T	p-B^{11}
t_c (ms)	6.192	5.707	1.429	0.002
$\dot{m}_{ex}$ (kg/s)	1.489	1.009	4.029	3.174
w (km/s)	5212	10473	10252	4563
F (kg-m/s^2)	7761864	10564393	41300388	14771881
γ	0.001	0.000	0.005	0.000
α_l	0.291	0.125	0.004	0.568
P_T (GW)	28590	63215	213728	34370
a_0 (km/s^2)	0.003	0.004	0.017	0.006
u_n (km/s)	11967	24004	23500	10684
X_T (km)	2020066554	1482820871	379316083	1061506143
MT (years)	107	54	55	119

The mission profile to Proxima b using the FDR is visualized in Figure 3.4.

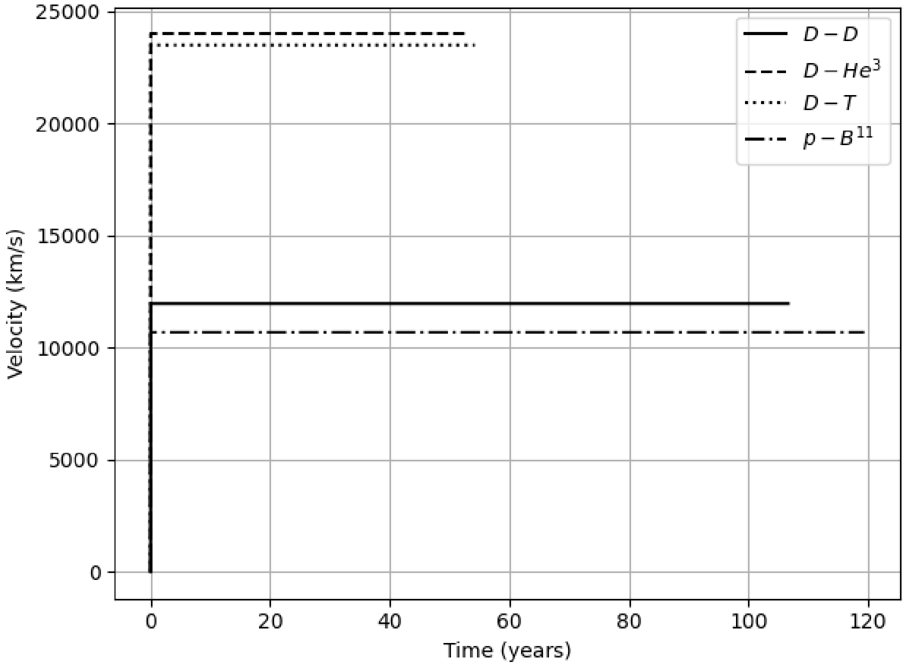

Figure 3.4: FDR flight profiles to Proxima b

The FDR was approximated to complete a single flyby mission to Proxima b in 54 years using D-He^3, or 55 years using D-T. The lower reactivities and energy products of D-D and p-B^{11} resulted in mission times longer than a century, with arrival speeds less than half that of other fuels. Therefore, while prioritizing the mission time, D-He^3 and D-T fuels are the most ideal for applications of the FDR.

3.4 IEC Device

Considering an IEC device in a spherical configuration with a confining magnetic field placed in a spacecraft of user-defined geometry, high power densities from a compact device may be achieved. Recall from Section 3.1.4 the fundamental properties of IEC devices and its limitations. This section uses methods from Rider[20] and makes the following key assumptions:

- Regions outside of the potential well have negligible collision-related effects.
- In the region of appreciable density:
  - The temperature and energy are uniform
  - Isotropic velocity distributions
  - Angular momentum of the velocity-space diffusion is negligible
  - The fuel ratio is constant throughout the region
  - Quasineutrality is maintained

Important characteristics of each fuel were defined with reactivity from the model in Section 3.2.1.

Table 3.6: IEC Design Parameters

	D-D	D-He^3	D-T	p-B^{11}
T' (keV)	100	70	20	300
$<\sigma v>_{1,2}$ (10^{-16} cm^3/s)	0.5007	1.087	4.341	2.576
n_0 (10^{17} cm^{-3})	10	5	5	5
y	0.5	0.5	0.5	0.167
ϵ	0.00097	0.00393	0.00377	0.00078
r_{core} (cm)	2.5	2.5	1.5	3
Q (MeV)	3.7	18.3	17.6	8.7
N_{cusp}	8	8	8	8
k_H	2	2	2	2
$\eta_{e,i}$	0.99	0.99	0.99	0.99
μ_i	2	2	2	2
E_{well} (keV)	300	210	60	900

The total fusion power before losses was determined using the reaction energy product (Q), fuel species ratio ($x = n_1/n_2$), and the core radius (r_{core}).

$$P_{fus}\ (W) = 2.68 \times 10^{-18} < \sigma v >_{1,2} Q \frac{x}{(x+Z_2)^2} n_0^2 r_{core}^3 \tag{3.35}$$

The performance of the IEC system assuming negligible synchronization radiation and Maxwellian distribution of electrons was determined using the same methodology as Section 3.3 from Spencer[49].

Table 3.7: IEC performance analysis results.

	D-D	D-He^3	D-T	p-B^{11}
t_c (ms)	6.192	5.707	1.429	1.929
$\dot{m}_{ex}$ (g/s)	0.35	0.24	0.21	0.13
w (km/s)	5212	10473	10252	4563
F (kg-m/s^2)	184	250	211	605
P_T (GW)	1.939	2.313	4.319	2.027
a_0 (km/s^2)	0.014	0.117	0.095	0.032
u_n (km/s)	16483	16483	16483	16483
X_T (km)	234262579235	117212078702	138811166484	84205392614
MT (years)	83	78.6	78.8	80

The mission to Proxima b using the IEC device is visualized in Figure 3.5.

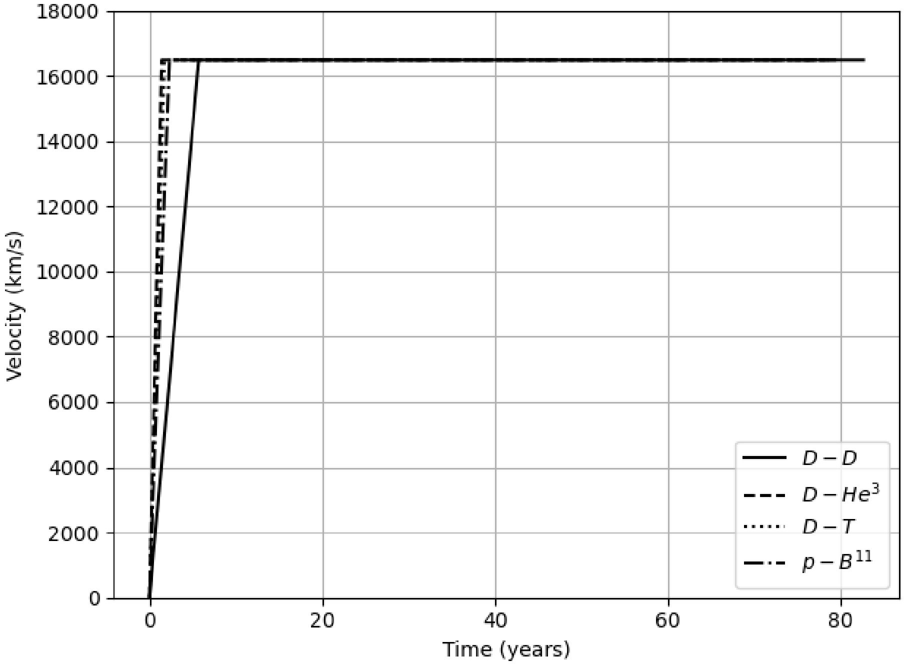

Figure 3.5: IEC flight profiles to Proxima b

The mission duration for the IEC was more balanced between the four fuels compared to the FDR while still favoring D-He^3 and D-T. The IEC device has an exhaust flow rate significantly less than the FDR due to its smaller exhaust flow area, but the propulsion time is much longer. Though the D-D and p-B^{11} fuels have a shorter mission time using the IEC device, the design assumes that there are no losses from the electron cusp confinement structure.

3.4.1 IEC Losses and Feasibility

To quantify the magnitude of losses from the IEC device, three confinement options were considered: electron cusp, electron grid, and ion grid. Assumptions were made for the radius edge ($r_e = 50r_{core}$) and the total radius ($r = 2r_e$), and losses were evaluated using methods from Rider[20]. Losses from electrons escaping from the confining mechanism of electron cusps varies depending on whether the fusion power is maximized ($x = Z_2$) and assumes that the edge of the plasma has $\beta = 1$.

$$P_{e\ loss\ cusp}\ (W) = \begin{cases} 6.26 \times 10^{18} P_{fus} N_{cusp} k_H^2 Z_2 \frac{E_{well}^{3/2}}{<\sigma v>_{1,2} Q n_0^2 r_{core}^3} & \text{if } x = Z_2 \\ 1.56 \times 10^{18} P_{fus} N_{cusp} k_H^2 \frac{(x+Z_2)^2}{x} \frac{E_{well}^{3/2}}{<\sigma v>_{1,2} Q n_0^2 r_{core}^3} & \text{if } x \neq Z_2 \end{cases} \tag{3.36}$$

Losses by using an electron grid instead of electron cusps make the assumptions that the electron energy, velocity, and density are evaluated at a grid of radius ($r_{grid} = r$) and (η_e) transparency to electrons.

$$P_{e\ loss\ grid}\ (W) = \begin{cases} 1.78 \times 10^{8} P_{fus} Z_2 (1-\eta_e) \frac{r_{grid}}{r_e} \frac{E_{well}^{3/2}}{<\sigma v>_{1,2} Q n_0 r_{core}} & \text{if } x = Z_2 \\ 1.19 \times 10^{-10} P_{fus} (1-\eta_e) r_{grid}^2 n_0 \left(\frac{r_c}{r_e}\right)^2 E_{well}^{3/2} & \text{if } x \neq Z_2 \end{cases} \tag{3.37}$$

Implementing, instead, an electrostatic grid that absorbs the power of electrons rather than the ions, the losses from the ion grid will similarly assume that the energy, velocity, and density are evaluated at a grid of radius ($r_{grid} = r$) and (η_i) transparency to ions.

$$P_{i\ loss\ grid}\ (W) = 2.79 \times 10^{-12} (1-\eta_i) r_{grid}^2 n_0 \left(\frac{r_c}{r_e}\right)^2 \frac{E_{well}^{3/2}}{\sqrt{\mu_i}} \tag{3.38}$$

The power losses from each confinement structure are summarized in Table 3.8.

Table 3.8: IEC system loss mechanisms.

	D-D	D-He^3	D-T	p-B^{11}
Electron Cusps Power Loss (GW)	22	13	2	11
Electron Grid Power Loss (GW)	4899104	1431482	78874	18328675
Ion Grid Power Loss (GW)	81042	23732	1305	303197
Total Fusion Power (GW)	1.9	2.3	4.3	2.0

The loss comparison from the 3 configurations indicates that the electron and ion grids exhibit an escape power significantly higher than the total fusion power. Electron cusps are the most promising option for confinement; however, work still needs to be done before IEC devices can sustain a net-gain.

3.5 Antimatter Initiated Microfusion

Antimatter Initiated Microfusion (AIM) uses a Penning trap to confine a cloud of antiprotons, then injects droplets of fuel mixed with a 2% admixture of U^{238} to aid with annihilation[21]. The fission fragments are not radioactive and do not require additional radiation shielding[13]. It is important to note that due to the unreasonably high antimatter mass requirements for the other fuels, only D-T and D-He^3 were considered for the AIM system.

Important characteristics of each fuel were defined with reactivity from the model in Section 3.2.1, and design choices from Gaidos et al[21].

Table 3.9: AIM Design Parameters

	D-He^3	D-T
T' (keV)	100	100
$< \sigma v >_{1,2}$ (10^{-16} cm^3/s)	1.729	8.433
n_0 (10^{17} cm^{-3})	6	6
y	0.5	0.5
ϵ	0.00393	0.00377
r_{core} (cm)	0.4	0.4
r (cm)	0.8	0.8
Q (MeV)	18.3	17.6
I_{sp} (s)	67000	61000
η_{eff}	0.84	0.69
β	100000	61000

Calculations for the thrust and exhaust power and its components use the same method from Sections 3.3 and 3.4. The analysis for the masses in this section use methods from Schmidt et al[12]. The mass ratio was determined using

$$MR = \left(\frac{1 + \Delta V / c}{1 - \Delta V / c} \right)^{\frac{c}{2w}} \tag{3.39}$$

Then the initial mass can be found assuming the structure to propellant mass ratio (λ) of 0.2.

$$M_F = \frac{M_{PL}}{1 + \lambda - (\lambda \ MR)} \tag{3.40}$$

The structural mass was found using Equation 3.16, and in result, the propellant mass is

$$M_P = \frac{M_S}{\lambda} \tag{3.41}$$

The Lorentz-Fitzgerald contraction factor (γ_{LF}) accounts for the change in dimension of the antimatter in the direction parallel to its motion.

$$\gamma_{LF} = \frac{1}{\sqrt{1-(w/c)^2}} \tag{3.42}$$

The antimatter mass is highly dependent on the performance of the AIM device and is a function of γ_{LF}.

$$M_a = \frac{M_{PL}}{2(1+\beta)} \frac{\gamma_{LF}-1}{\gamma_{LF}+(\eta_{eff}-1)} \frac{MR-1}{1+\lambda-\lambda\ MR} \tag{3.43}$$

The masses for system components using an AIM propulsion system is summarized in Table 3.10.

Table 3.10: AIM mass results

	D-He^3	D-T
M_I (kg)	10441	12626
M_F (kg)	2157	2521
M_s (kg)	1657	2021
M_a (g)	0.030	0.194
$M_{P,fus}$ (kg)	82843	10105
$M_{P,T}$ (kg)	82843	10105

Characterization of the performance for a device employing AIM was based on methods from Borowski[52]. The total mission time using AIM can be calculated using

$$t_{AB} = \frac{I_{sp}}{F/W_F}\frac{1}{C_2}\left(\frac{1}{C_1} - 1\right) = MT\ (s) \tag{3.44}$$

The constants used in Equation 3.44 can be found by solving the following system of equations

$$D_{AB} = \frac{g_0 I_{sp}^2}{F/W_F}\left(\frac{1}{C_2}\right)\left(\frac{1}{C_1} - 1\right)^2 = D_{BA} \tag{3.45}$$

$$D_{BA} = \frac{g_0 I_{sp}^2}{F/W_F}\left(\frac{1}{C_2} - 1\right)^2 \tag{3.46}$$

Results from the analysis were represented in Table 3.11.

Table 3.11: AIM performance analysis results

	D-He^3	D-T
t_c (ms)	2.144	2.144
$\dot{m}_{ex}$ (g/s)	0.002	0.009
w (km/s)	10473	10252
F (kg-m/s^2)	19	90
P_T (GW)	103210499	472208032
a_0 (m/s^2)	0.002	0.009
u_n (km/s)	16500	16500
X_T (km)	23740772894	5027735926
MT (years)	72	71

The AIM system employing both fuels had a mission time of at most 72 years, slightly favoring D-T due to its higher reactivity under the same driver conditions. The flight profile for each fuel is visualized in Figure 3.6.

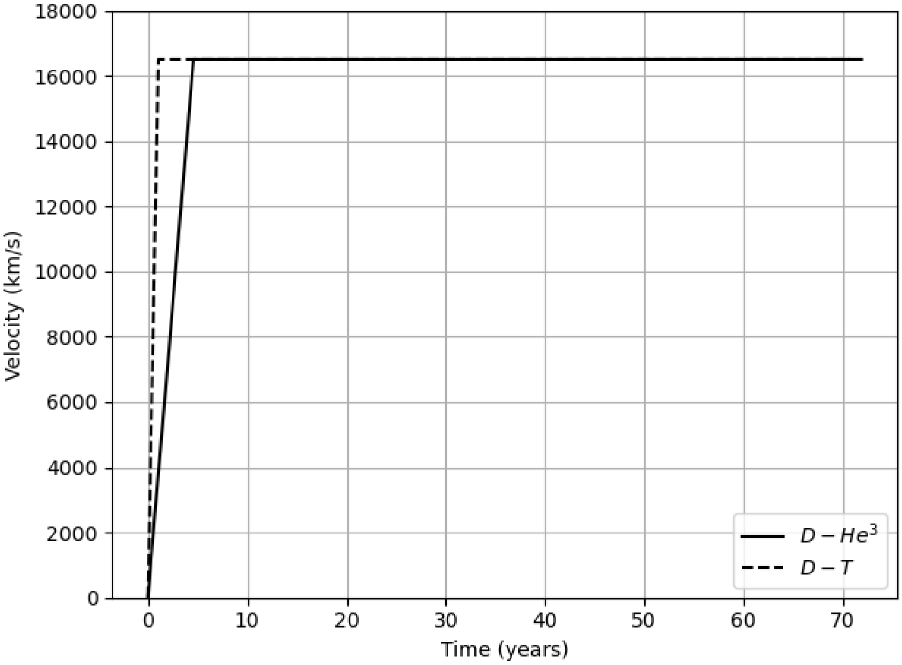

Figure 3.6: AIM flight profiles to Proxima b

However, since D-T has a lower energy utilization factor, it will require a higher amount of antimatter, making it less favorable than using the D-He^3 fuel. Though mission time is a preferred statistic for the overall performance of a propulsion system, the difficulty of antimatter sourcing makes D-He^3 the preferred fuel for the AIM device.

3.6 Performance Comparison

To directly compare the performance of each propulsion system, the payload ratio and mission time are evaluated.

The payload ratio ($\frac{M_{PL}}{M_I}$) is an indicator for the efficiency of the spacecraft. While the IEC system has a much higher payload ratio at approximately 20%, the losses due to the efficiency of the confinement structure may significantly affect the final result, with more mass being used to support the IEC. AIM has a reasonable payload ratio due to the low demands of the system while maintaining its performance.

Table 3.12: Payload ratio for each propulsion system and fuel

	FDR	IEC	AIM
D-D	0.0002	0.04	
D-He^3	0.0002	0.21	0.05
D-T	0.0002	0.20	0.04
p-B^{11}	0.0002	0.03	

A shorter mission time allows for the collected data to be relayed earlier and reduced operational costs. The FDR results in the shortest mission length for the fuels with the highest energy output: D-T and D-He^3. If the simpler D-D fuel or aneutronic p-B^{11} fuel were preferred, the IEC system would be more suitable, disregarding its potential losses.

Table 3.13: Mission time (years) for each propulsion system and fuel

	FDR	IEC	AIM
D-D	107	83	
D-He^3	54	78.6	72
D-T	55	78.8	71
p-B^{11}	119	80	

Overall, the AIM system provides the most ideal payload ratio at a reasonable mission time. The FDR, however, is more advantageous due to its shorter mission time and better resource accessibility. The IEC system faces severe technical challenges but, once addressed, may have a similar performance to the analysis in Section 3.4.

The fuels with a higher energy product resulted in better performance for both mission time and payload ratio. Though D-T is relatively easier to ignite and sustain, the D-He^3 fuel provides a more promising mission performance. D-He^3 also avoids the added mass, volume, and cost constraints associated with tritium and neutron management, making it the most ideal for fusion propulsion.

Chapter 4

Trajectory Analysis

A straight flight path from Earth to Proxima b is reasonable considering the scale of the propulsion system performance. Three flight profiles for the approach to Proxima b were considered: fast flyby, slow flyby, and bounded orbit.

4.1 Single Fast Flyby

The fast flyby scenario assumes a short boost phase with constant acceleration of the spacecraft, then coast through the interstellar medium to Proxima b. The analysis in Chapter 3 demonstrates the expected mission times and flyby speeds for an unregulated flight. Mission times for the fast flyby scenario, represented in Table 3.13, was in the range of 54-119 years. The expected velocities, summarized in Table 4.1, are on the scale of 10^4 km/s.

Table 4.1: Burnout velocity (u_n, in km/s) for each propulsion system and fuel

	FDR	IEC	AIM
D-D	11967	16483	
D-He^3	24004	16483	16500
D-T	23500	16483	16500
p-B^{11}	10684	16483	

At such high velocities, the instrumentation aboard the spacecraft will very likely not be able to collect reasonable data. The spacecraft would be within the minimum altitude range required by the instrumentation for only a couple of seconds, at most. The likelihood of the spacecraft remaining within the lensing region of Alpha Centauri long enough for the communications system to relay a bulk of the vital data back to the receiver probe would be very low. Therefore, to ensure that sufficient data is collected by the science payload and relayed back to Earth, it is essential to have the spacecraft slow down prior to its approach phase of Proxima b.

4.2 Single Slow Flyby

The practicality of certain propulsion methods for a mission requiring deceleration is at risk due to the time restrictions for storage of antiprotons and tritium. Engaging the propulsion system even as soon as halfway through the flight would completely disqualify the AIM system due to its limited antiproton storage time. Additionally, storing the tritium so that it does not decay after its half-life of 12.3 years would be expensive in mass, volume, power, and cost. If the mission time were to remain less than 100 years, the only reasonable candidate for this mission would be the FDR employed with D-He^3 fuel.

For a single slow flyby, the instrumentation specifications govern the ideal speed at which the spacecraft should approach Proxima b. Considering that a bulk of the instrumentation was in reference to the Europa Clipper mission, then the desired flyby speed should be approximately 25 km/s. By rotating the spacecraft to decelerate, the FDR can use the same propulsion system by re-injecting fuel into the thrust structure, resulting in deceleration at an averaged constant rate of 4 m/s^2 (Table 3.5). Then the deceleration phase would begin at approximately 1.5×10^9 km from Proxima b, determined using Equation 3.32.

The updated propellant requirements were determined using the system of equations from Section 3.3. Since during deceleration, the spacecraft assumes the same initial conditions provided during the fast flyby analysis, the propellant mass for deceleration is 2435119 kg. This propellant acts as second payload mass (M_{PL2}) during the boost phase, since the spacecraft will need to store it until it is within 10^9 km of Proxima b. Using the code in Appendix B, the deceleration propellant mass was added to the payload mass then rerun to determine the resultant masses, demonstrated in Table 4.2.

Table 4.2: FDR masses for slow flyby of Proxima b at 25 km/s using D-He^3 fuel

M_I (kg)	387411010
M_F (kg)	38958567
M_S (kg)	8687525
M_P (kg)	348452442
M_{PL2} (kg)	2435119
f (s^{-1})	0.140
P_{SEP} (kW)	32841

The performance analysis from Section 3.3 was rerun with the new masses using methods from Spencer[49]. The key results, including the distance traveled and duration of each phase, are represented in Table 4.3.

Table 4.3: FDR Performance for slow flyby of Proxima b at 25 km/s using D-He^3 fuel

	Acceleration Phase	Coast Phase	Deceleration Phase
a_0 (km/s^2)	0.00003	0.000	0.004
u_n (km/s)	24004	24004	25
X (km)	211751370952	39830864705173	72023923875
t (years)	3.758	52.862	0.190

Due to the increased mass of the spacecraft during the boost phase, more thrust is needed to maintain the performance of the FDR. However, since the design of the system is not governed by the amount of fuel that is provided, the thrust will remain approximately the same, resulting in decreased acceleration proportional to the additional propellant mass required. Therefore, the constant acceleration during the boost phase is only $0.0075a_0$ compared to Section 3.3. The amount of propellant provided increases the acceleration time of the spacecraft to slightly more than 3.75 years before coasting for 52.9 years to the target deceleration region, as shown in Figure 4.1.

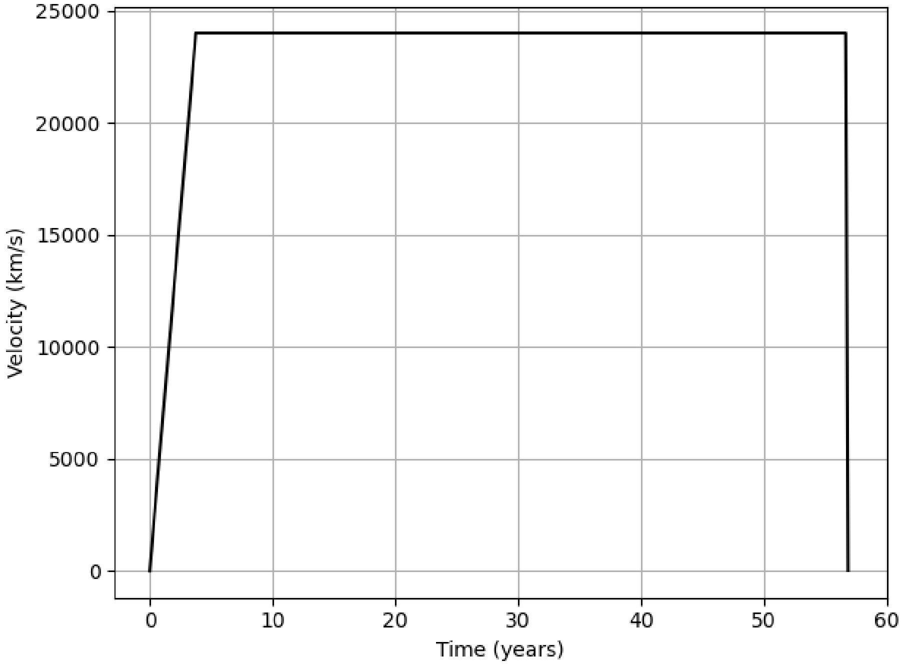

Figure 4.1: FDR flight profile for a slow flyby of Proxima b

The masses of the spacecraft at the end of the coast phase, after exhausting the acceleration propellant mass, now align with those in Table 3.3. The spacecraft can decelerate rapidly for a shorter distance, similar to Section 3.3, until it reaches a flyby speed of 25 km/s. The performance for the slow flyby scenario demonstrates a total mission duration of approximately 57 years.

4.3 Bounded Orbit

Considering the properties of Proxima b from Section 1.1 and ideal flyby altitudes for the instrumentation in Chapter 2, boundary conditions for the bounded orbit scenario are defined. For an orbit insertion of the exoplanet, the spacecraft must decelerate from the coasting speed to 46.5 km/s. The updated mission profile, represented in Table 4.4, was determined using the code from Appendix B and methods from Spencer[49].

Table 4.4: FDR Performance for bounded orbit of Proxima b at 46.5 km/s using D-He^3 fuel

	Acceleration Phase	Coast Phase	Deceleration Phase
a_0 (km/s^2)	0.00003	0.000	0.004
u_n (km/s)	24004	24004	47
X (km)	211751370952	39830864897329	72023731719
t (years)	3.758	52.766	0.190

The values closely align with those from Table 4.3 since the deceleration speed is in the same order of magnitude as Section 4.2. The deceleration phase is slightly shorter in distance, but the effect of changes to the burnout velocity on mission time is insignificant for the overall performance analysis, as shown in Figure 4.2.

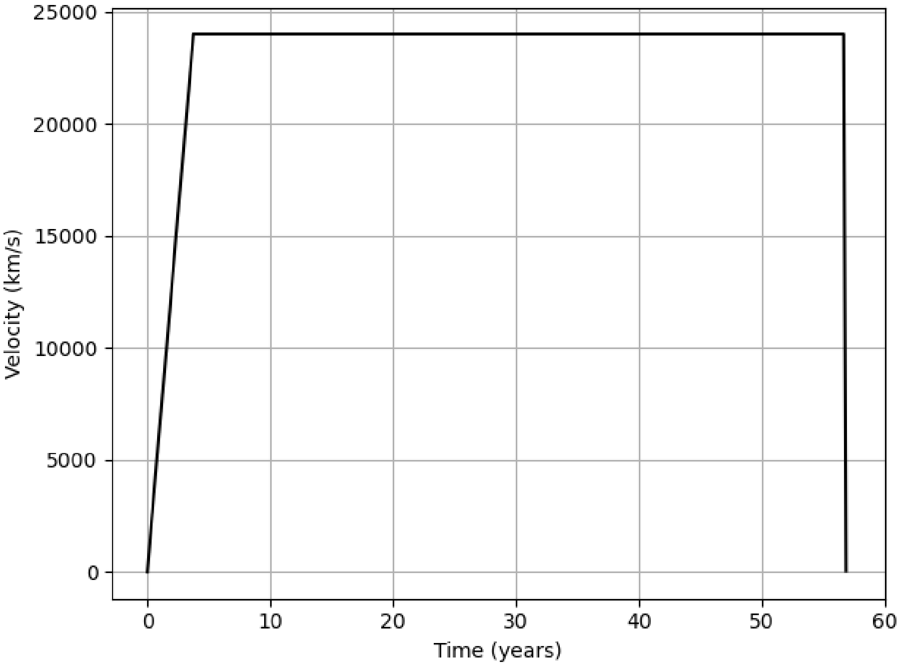

Figure 4.2: FDR flight profile for an orbit insertion about Proxima b

The deceleration time, however, is not insignificant for orbit insertion since changes to the final velocity on the km/s scale is proportional to the propulsion time on the minutes scale such that each additional minute of propulsion can vary the burnout velocity by ~2 km/s.

4.4 Interstellar Dust

For a spacecraft traveling through the interstellar medium, impacts from dust particles need to be considered. The analysis will assume a particle matter density (ρ_d) of 2.57×10^{-27} g/cm^3 and a mean dust particle mass (m_d) of 2×10^{-12} g [53]. The impact frequency (f) for the spacecraft as a function of the shielding area (A_0) is

$$f \text{ (impacts/s)} = \frac{A_0 L(\rho_d/m_d)}{MT} \tag{4.1}$$

One can consider the impact of dust collisions based on a specified desired shielding area, represented in Figure 4.3.

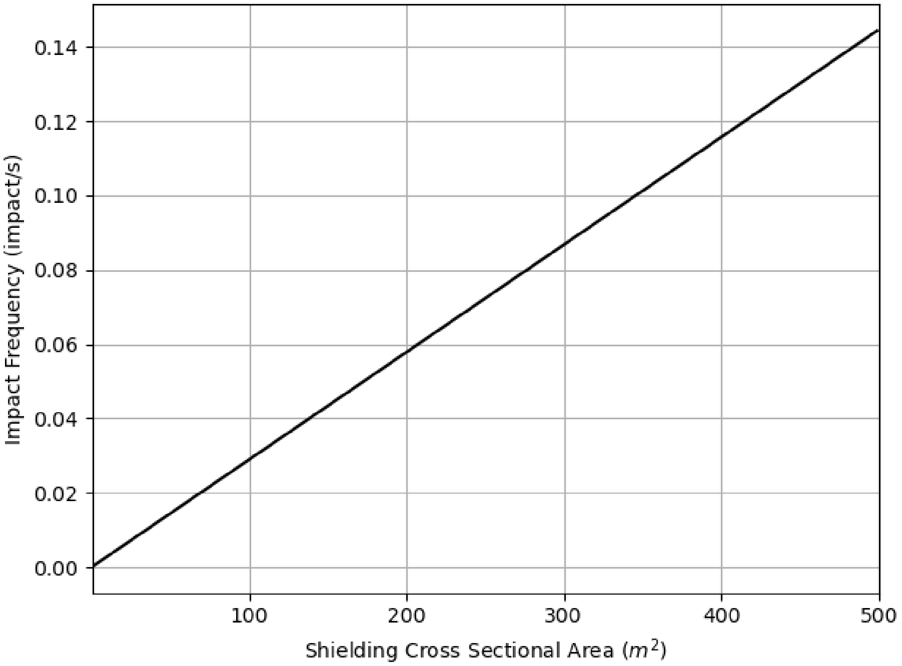

Figure 4.3: Dust impact frequency as a function of shielding area

To further quantify the collision influence on the spacecraft, the total energy deposition (E_k) throughout the mission is considered as a function of the shielding material density (ρ), shielding thickness (δ), mean dust particle radius (r), and spacecraft velocity[54].

$$E_k = \frac{1}{2}\frac{A_0 L \rho_d}{m_d}\rho\pi r^2 \delta v^2 \tag{4.2}$$

Spacecraft shielding can either be multi-layered or consist of a single species, such as Boron, Polyethylene, and Kevlar. Two basic options, Lithium and Aluminum, were considered to demonstrate the effect of shielding conditions on the energy deposition of particles.

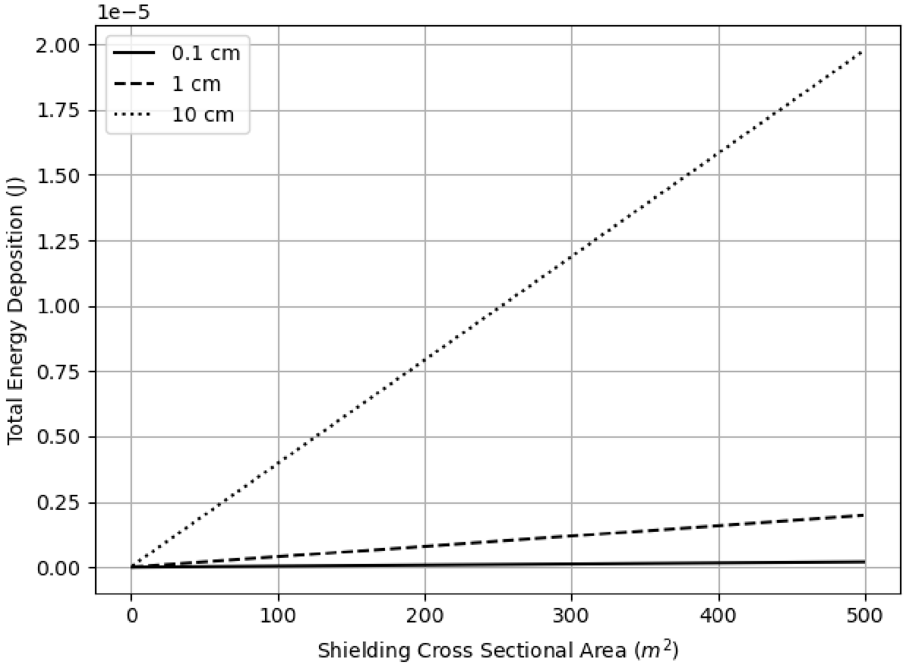

Figure 4.4: Total energy deposition from dust on a Lithium shield of varying cross sectional area and thicknesses

The total energy deposition from dust collisions throughout the mission is less than 2×10^{-5} J for a range of shielding parameters, as demonstrated in Figure 4.4.

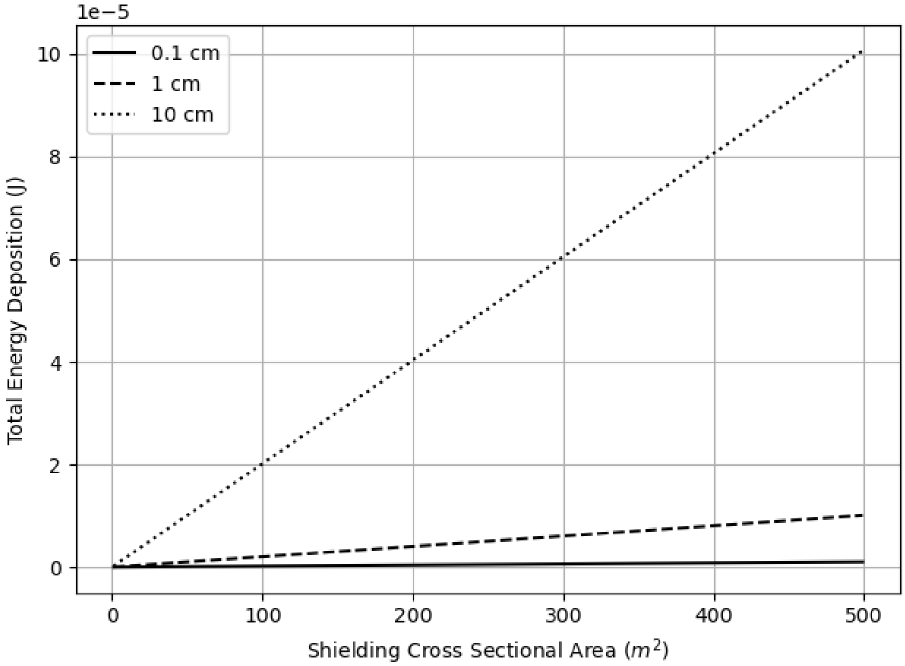

Figure 4.5: Total energy deposition from dust on a Aluminum shield of varying cross sectional area and thicknesses

Aluminum acts as a more effective shielding material, absorbing more of the impacting energy from the dust particle than Lithium, as demonstrated in Figure 4.5. Using the spacecraft conditions for the single slow flyby and multiple flyby scenarios, the total slowing energy should be significantly less than that provided by the propulsion system. Adequate shielding for the spacecraft was a general assumption for this work; however, the specific shielding thickness, material, and size will ultimately determine the survivability of the spacecraft with respect to impacting dust.

Chapter 5

Conclusions

In this study, framework for a large-scale spacecraft using fusion propulsion was explored for a mission to Proxima b. Specifications for the science payload provided boundary conditions for three propulsion systems on three flight scenarios to the exoplanet.

Instrumentation The primary objective of the instrumentation for this mission was to investigate the habitability of Proxima b. Due to the properties of Proxima b (Section 1.1) and the nature of the mission, the instruments were selected in reference to several missions that conduct investigations using single or multiple flybys, some of which use additional preparation for harsh radiation conditions, such as Europa Clipper. The instruments collectively provide an in-depth analysis of the structure, composition, and activity of Proxima b, with only the magnetometer changing between the single and multiple flyby scenarios. The data collection for most instruments is more effective for the bounded-orbit scenario with multiple flybys; however, they would still collect sufficient data during a single flyby.

Communication of the data (Section 2.11) takes advantage of solar gravitational lensing to send data at an ideal rate of 10 Mb per second per Watt. The science payload uses less than 394 W of power with a large data volume; however, the data that is relayed back to Earth can be reduced by using a machine learning algorithm to filter useful data. The total payload mass provides a boundary condition for the propulsion analysis, where the total mass of the payload was less than 336 kg. To account for additional components, such as optional radiators and radiation shielding, the payload mass was rounded to 500 kg.

Propulsion System A background was provided on the four main types of fusion environments with their notable advantages and disadvantages. Magnetic and inertial confinement are the most technologically developed, but their large mass and capacity makes it inapplicable for spacecraft. Using concepts from both confinement systems, magneto-inertial fusion provides a more compact solution by relieving the powerful driver requirements. Inertial electrostatic confinement similarly has a high energy output for a compact and lightweight device, but suffers major technical challenges as demonstrated in Section 3.4.1. Antimatter annihilation provides the highest energy output with a compact system; however, it is very difficult to source a sufficient amount of antiprotons. The driver required to induce fusion conditions can be replaced by a very lightweight and compact Penning trap, using antimatter annihilation to induce a fusion reaction, providing the ultimate solution to the unreasonable scale of antiproton mass requirements and compactness of fusion propulsion systems.

The performance of each fuel was governed by the average reactivity at certain temperatures, quantified in Section 3.2.1. While D-D is easiest to source naturally, it has the lowest peak reactivity and energy output (~11 MeV) of all the fuels. D-He^3 is not only advantageous for its aneutronic nature, but it also has a high energy output per fusion event (18.3 MeV). However, since its peak reactivity is not as high as D-T, the total fusion energy and performance from a D-He^3 fuel may be lower than D-T (17.6 MeV). The sourcing and management of tritium puts D-T at a disadvantage, but its high peak reactivity at a lower temperature makes it easier to ignite and sustain fusion conditions. Finally, the aneutronic nature and easy sourcing of p-B^{11} makes it ideal in principle, but it has a lower energy output (8.68 MeV) and requires a very high temperature to reach its peak reactivity value.

Section 3.3 outlined the performance of the fusion driven rocket using each fuel, where the lowest mission times (~55 years) were provided by D-He^3 and D-T. The IEC suffers from significant losses from the confinement system, as demonstrated in Section 3.4.1. However, further development of the electron cusps would make IEC the preferred propulsion system for D-D or p-B^{11} fuels ($MT \leq 83$ years). The IEC optimized the payload ratio at the cost of a longer mission time ($MT \approx 79$ years) for D-He^3 and D-T fuels. Section 3.5 showed that the AIM device provided the best compactness and reduced structural mass while sacrificing mission time ($MT \leq 72$ years). Regardless, AIM had a shorter mission time than IEC while maintaining a reasonable payload ratio.

Trajectory Analysis Considering the spacecraft altitude and velocity requirements of the instrumentation, a single fast flyby was unreasonable to collect data, with speeds on the scale of 10^4 km/s. The spacecraft would need a deceleration phase, for which the FDR employed with D-He^3 was the only feasible option. Section 4.2 described the modified analysis of Section 3.3, resulting in a total mission time less than 57 years. Alternatively, Section 4.3 examined the mission profile for a bounded orbit scenario, where the deceleration at burnout allows for orbit insertion, resulting in a slightly reduced propulsion distance for this phase. The mission time was less than 57 years, with a variation on the scale of minutes compared to the slow flyby scenario. Challenges that come with pointing accuracy may imply a slightly higher propellant mass to account for course correction needs. The propulsion system allows for multiple burns by additional fuel injection without significant changes to the overall mission time. A basic analysis on the effects of impacting interstellar dust on the shielding area, thickness, and material showed a low impact frequency with a slowing energy significantly smaller than that provided by the propulsion system.

Final Remarks This work provided a foundation for applications of fusion propulsion on large scale spacecraft traveling extreme distances. The propulsion system analysis was based on the current state of research for each device. The omitted losses and assumptions made for each system may slightly alter the actual performance; however, the conclusions should still align with the work from this paper. Considerations for the relay of data from the Proxima b spacecraft to Earth will ultimately govern the effectiveness of this mission, and should be explored in future work. Lastly, guidance of the spacecraft at extreme distances should be addressed by using an automated system to detect issues and make reasonable decisions. Pairing of the guidance system with optical navigation technologies will allow for the spacecraft to assess necessary corrections. Assuming that the spacecraft is able to communicate from Alpha Centauri and operate using a self-sufficient guidance and navigation system, a mission to Proxima b within 60 years using a large-scale spacecraft is possible.

Bibliography

[1] Litchford, R. A. and Sheehy, J. A. "Prospects for Interstellar Propulsion". In: *Annual AAS Guidance, Navigation and Control Conference* (2020). URL: https://ntrs.nasa.gov/citations/20200000759.

[2] Ribas, gnasi et al. "The habitability of Proxima Centauri b". In: *Astronomy Astrophysics* 596.A111 (2016). DOI: 10.1051/0004-6361/201629576.

[3] Parkin, K. L. "The Breakthrough Starshot system model". In: *Acta Astronautica* 152 (Nov. 2018), pp. 370–384. ISSN: 0094-5765. DOI: 10.1016/j.actaastro.2018.08.035. URL: http://dx.doi.org/10.1016/j.actaastro.2018.08.035.

[4] Millis, M. G., Greason, J., and Stevenson, R. "Breakthrough Propulsion Study: Assessing Interstellar Flight Challenges and Prospects". In: ().

[5] Kritcher, A. L. et al. "Design of first experiment to achieve fusion target gain > 1". In: *Physics of Plasmas* 31.7 (July 2024), p. 070502. ISSN: 1070-664X. DOI: 10.1063/5.0210904. eprint: https://pubs.aip.org/aip/pop/article-pdf/doi/10.1063/5.0210904/20171807/070502_1_5.0210904.pdf. URL: https://doi.org/10.1063/5.0210904.

[6] Anglada-Escudé, G. et al. "A terrestrial planet candidate in a temperate orbit around Proxima Centauri". In: *Nature* 536.7617 (2016), pp. 437–440. ISSN: 1476-4687. DOI: 10.1038/nature19106. URL: http://dx.doi.org/10.1038/nature19106.

[7] Laboratory, J. H. U. A. P. URL: https://hub.jhu.edu/magazine/2021/spring/apl-interstellar-probe/.

[8] Turbet, M. et al. “The habitability of Proxima Centauri b”. In: *Astronomy Astrophysics* 596.A112 (2016). DOI: `10.1051/0004-6361/201629577`.

[9] Coleman, E. K. 2016. URL: `https://www.eso.org/public/images/eso1629c/`.

[10] Stephen R. Kane, D. M. G. and Turnbull, M. C. “ON THE ORBITAL INCLINATION OF PROXIMA CENTAURI b”. In: *The Astronomical Journal* 153.2 (2017). DOI: `10.3847/1538-3881/153/2/52`.

[11] Agency, I. A. E. *Fusion*. 2025. URL: `https://www.iaea.org/topics/fusion`.

[12] Schmidt, G. R. et al. “Antimatter Requirements and Energy Costs for Near-Term Propulsion Applications”. In: *Journal of Propulsion and Power* 16.5 (2000). DOI: `10.2514/2.5661`.

[13] Gaidos, G et al. “Antiproton-catalyzed microfission/fusion propulsion systems for exploration of the outer solar system and beyond”. In: *AIP Conference Proceedings* 420.1 (Jan. 1998). ISSN: ISSN 0094-243X. DOI: `10.1063/1.54761`. URL: `https://www.osti.gov/biblio/21179671`.

[14] Winterberg, F. *Advanced Deuterium Fusion Rocket Propulsion For Manned Deep Space Missions*. 2009. arXiv: `0906.0740 [physics.plasm-ph]`. URL: `https://arxiv.org/abs/0906.0740`.

[15] Chapman, J. J. “Advanced fusion reactors for space propulsion and power systems”. In: *2011 Abstracts IEEE International Conference on Plasma Science*. 2011. DOI: `10.1109/PLASMA.2011.5992998`.

[16] Anderton, M. et al. “Novel high temperature tritium blanket designs for confined spaces in spherical tokamak fusion reactors”. In: *Fusion Engineering and Design* 210 (2025), p. 114732. ISSN: 0920-3796. DOI: `10.1016/j.fusengdes.2024.114732`.

[17] Tardini, A. G., Scott, J. H., and Miley, G. H. *NASA-NIAC 2001 PHASE I RESEARCH GRANT on Aneutronic Fusion Spacecraft Architecture Final Research Activity Report.* 2012. URL: https://www.nasa.gov/wp-content/uploads/2017/07/niac_2011_phasei_tardittianeutronicfusionspacecraftarchitecture_tagged.pdf.

[18] Hill, C. *Nuclear fusion cross sections and reactivities.* 2021. URL: https://scipython.com/blog/nuclear-fusion-cross-sections/.

[19] Slough, J. "The Fusion Driven Rocket". In: *2024 IEEE Aerospace Conference.* 2024, pp. 1–20. DOI: 10.1109/AERO58975.2024.10521025.

[20] Rider, T. H. "A general critique of inertial-electrostatic confinement fusion systems". In: *Physics of Plasmas* 2.6 (1995), pp. 1853–1872. DOI: 10.1063/1.871273.

[21] Gaidos, G. et al. "AIMStar: Antimatter initiated microfusion for pre-cursor interstellar missions". In: *AIP Conference Proceedings* 458.1 (Jan. 1999), pp. 954–959. ISSN: 0094-243X. DOI: 10.1063/1.57674. URL: https://doi.org/10.1063/1.57674.

[22] Paczkowski, B. et al. *Europa Clipper Instrument Summaries.* © 2022 Jet Propulsion Laboratory, California Institute of Technology. 2022. URL: https://example.com/ml-europa.pdf.

[23] Fountain, G. H. et al. "The New Horizons Spacecraft". In: *Space Sci Rev* 140 (2008), pp. 23–47. DOI: 10.1007/s11214-008-9374-8.

[24] Kivelson, M. G. et al. "The Europa Clipper Magnetometer". In: *Space Sci Rev* 219.48 (2023). DOI: 10.1007/s11214-023-00989-5.

[25] Kraus, H. and Cochrane, C. *SiC Magnetometer.* 2022. URL: https://microdevices.jpl.nasa.gov/capabilities/nano-and-micro-systems/sic-magnetometer/.

[26] Westlake, J. H. et al. “The Plasma Instrument for Magnetic Sounding (PIMS) on the Europa Clipper Mission”. In: *Space Sci Rev* 219.62 (2023). DOI: 10.1007/s11214-023-01002-9.

[27] Christensen, P. R. et al. “The Europa Thermal Emission Imaging System (E-THEMIS) Investigation for the Europa Clipper Mission”. In: *Space Sci Rev* 220.38 (2024). DOI: 10.1007/s11214-024-01074-1.

[28] Gladstone, R. et al. “The Ultraviolet Spectrograph (UVS) on ESA’s JUICE Mission”. In: *AAS/Division for Planetary Sciences Meeting Abstracts* 45 (2013). URL: https://ui.adsabs.harvard.edu/abs/2013DPS....4521104G/abstract.

[29] Gladstone, G. R. et al. “The Ultraviolet Spectrograph on NASA’s Juno Mission”. In: *Space Sci Rev* 213 (2017), pp. 447–473.

[30] Tyler, G. L. et al. “The New Horizons Radio Science Experiment (REX)”. In: *Space Sci Rev* 140 (2008), pp. 217–259. DOI: 10.1007/s11214-023-00972-0.

[31] Mazarico, E. et al. “The Europa Clipper Gravity and Radio Science Investigation”. In: *Space Sci Rev* 219.30 (2023). DOI: 10.1007/s11214-023-00972-0.

[32] Waite, J. H. et al. “MASPEX-Europa aboard Clipper: A mass spectrometer for investigating the habitability of Europa”. In: *EPSC-DPS Joint Meeting 2019* 13 (2019). URL: https://meetingorganizer.copernicus.org/EPSC-DPS2019/EPSC-DPS2019-559-1.pdf.

[33] Blaney, D. L. et al. “The Mapping Imaging Spectrometer for Europa (MISE)”. In: *Space Sci Rev* 220.80 (2024). DOI: 10.1007/s11214-024-01097-8.

[34] Blankenship, D. D. et al. “Radar for Europa Assessment and Sounding: Ocean to Near-Surface (REASON)”. In: *Space Sci Rev* 220.51 (2024). DOI: 10.1007/s11214-024-01072-3.

[35] Kempf, S. et al. “SUDA: A SUrface Dust Analyser for Compositional Mapping of the Galilean Moon Europa”. In: *Space Sci Rev* 221.10 (2025). DOI: 10.1007/s11214-025-01134-0.

[36] Cheng, A. F. et al. “Long-Range Reconnaissance Imager on New Horizons”. In: *Space Sci Rev* 140 (2008), pp. 189–215. DOI: 10.1007/s11214-007-9271-6.

[37] III, S. E. H. et al. “The Mercury Dual Imaging System on the MESSENGER Spacecraft”. In: *Space Sci Rev* 131 (2007), pp. 247–338. DOI: 10.1007/s11214-007-9266-3.

[38] Hippke, M. “Interstellar communication. II. Application to the solar gravitational lens”. In: *Acta Astronautica* 142 (Jan. 2018), pp. 64–74. ISSN: 0094-5765. DOI: 10.1016/j.actaastro.2017.10.022. URL: http://dx.doi.org/10.1016/j.actaastro.2017.10.022.

[39] CERN. *First atoms of antimatter produced at CERN*. 1996. URL: https://home.cern/news/press-release/cern/first-atoms-antimatter-produced-cern.

[40] Wu, J. *Measurements of cosmic ray antiprotons with PAMELA and studies of propagation models*. 2012. arXiv: 1205.5007 [astro-ph.HE]. URL: https://arxiv.org/abs/1205.5007.

[41] Koning, A. J. and Agency, I. A. E. *Evaluated Nuclear Data File (ENDF)*. Version ENDF/B-VIII.0. 2018. URL: https://www-nds.iaea.org/exfor/endf.htm.

[42] Friedman, I. “Deuterium content of natural waters and other substances”. In: *Geochimica et Cosmochimica Atca* 4 (1953), pp. 89–103. DOI: 10.1016/0016-7037(53)90066-0.

[43] Verkhovniy, A. I. et al. “Sources for Helium-3 Isotope Extraction and Prospects of its Development”. In: *Chem Petrol Eng* 57 (2022), pp. 940–951. DOI: 10.1007/s10556-022-01029-9.

[44] Environmental Protection, C. o. P. Department of. *FACTS ABOUT RADIOACTIVE TRITIUM*. 2025. URL: https://greenport.pa.gov/elibrary//PDFProvider.ashx?action=PDFStream&docID=14666&chksum=&revision=3&docName=FACTS+ABOUT+RADIOACTIVE+TRITIUM&nativeExt=pdf&PromptToSave=False&Size=219744&ViewerMode=2&overlay=0.

[45] ORGANIZATION, I. *Tritium Breeding*. 2023. URL: https://www.iter.org/machine/supporting-systems/tritium-breeding.

[46] Wang, Y. B. et al. "Economic estimation of boron isotope production by gas diffusion method using BF3 as processing gas". In: *Journal of Physics* 1696.012006 (2020). DOI: 10.1088/1742-6596/1696/1/012006.

[47] Lawson, J. D. "Some Criteria for a Power Producing Thermonuclear Reactor". In: *Proceedings of the Physical Society. Section B* 70.1 (1957), p. 6. DOI: 10.1088/0370-1301/70/1/303.

[48] Slough, J. T. et al. "Confinement and stability of plasmas in a field-reversed configuration". In: *Phys. Rev. Lett.* 69 (15 1992), pp. 2212–2215. DOI: 10.1103/PhysRevLett.69.2212.

[49] Spencer, D. F. *FUSION PROPULSION SYSTEM REQUIREMENTS FOR AN INTERSTELLAR PROBE*. Tech. rep. California. Inst. of Tech., Pasadena. Jet Propulsion Lab., 1963. URL: https://www.osti.gov/biblio/4684095.

[50] Glasstone, S. and Lovberg, R. H. *Controlled Thermonuclear Reactions*. D. Van Nostrand Co., 1960. ISBN: 9780442027162.

[51] Rose, D. and Jr., M. C. *Plasmas and Controlled Fusion*. The MIT Press, 1961. ISBN: 9780262180061.

[52] Borowski, S. K. “A comparison of fusion/antiproton propulsion systems for interplanetary travel”. In: *23rd Joint Propulsion Conference*. American Institute of Aeronautics Astronautics, Inc., 1987. DOI: `10.2514/6.1987-1814`. URL: `https://arc.aiaa.org/doi/abs/10.2514/6.1987-1814`.

[53] Draine, B. T. “Physics of the Interstellar and Intergalactic Medium”. In: *Princeton Series in Astrophysics* (2011). DOI: `10.1016/j.actaastro.2018.08.035`.

[54] Long, K. F. *Calculations of Particle Bombardment due to Dust and Charged Particles in the ISM on the Project Starshot Gram-Scale Interstellar Probe*. 2023. arXiv: `2307.12160 [physics.space-ph]`. URL: `https://arxiv.org/abs/2307.12160`.

Appendices

Appendix A

Reactivity

(Adapted from Hill[18])

```
import numpy as np
from matplotlib import rc
import matplotlib.pyplot as plt
from scipy.constants import e, k as kB
from scipy.integrate import quad
from cycler import cycler


# To plot using centre-of-mass energies instead of lab-fixed energies
COFM = True

# To plot using different linestyles (pdf-friendly readibility)
linestyle_cycler = cycler('linestyle',['-','--',':','-.'])
plt.rc('axes', prop_cycle=linestyle_cycler)

# Reactant masses in atomic mass units (u).
u = 1.66053906660e-27
```

```
masses = {'D': 2.014, 'T': 3.016, '3He': 3.016, '11B': 11.009305167,
          'p': 1.007276466620409}

# Energy grid, 1 - 100,000 keV, evenly spaced in log-space.
Egrid = np.logspace(0, 5, 1000)

class Xsec:
    def __init__(self, m1, m2, xs):
        self.m1, self.m2, self.xs = m1, m2, xs
        self.mr = self.m1 * self.m2 / (self.m1 + self.m2)

    @classmethod
    def read_xsec(cls, filename, CM=True):
        # Read in the cross section (in barn) as a function of energy (MeV).
        E, xs = np.genfromtxt(filename, comments='#', skip_footer=2,
                              unpack=True)
        if CM:
            collider, target = filename.split('_')[:2]
            m1, m2 = masses[target], masses[collider]
            E *= m1 / (m1 + m2)

        # Interpolate the cross section onto the Egrid (keV) and
        # convert from barn to cm2.
        xs = np.interp(Egrid, E*1.e3, xs*1.e-28)
        return cls(m1, m2, xs)

```

```
    def __add__(self, other):
        return Xsec(self.m1, self.m2, self.xs + other.xs)

    def __mul__(self, n):
        return Xsec(self.m1, self.m2, n * self.xs)
    __rmul__ = __mul__

    def __getitem__(self, i):
        return self.xs[i]

    def __len__(self):
        return len(self.xs)

xs_names = {'D-T': 'D_T_-_a_n.txt',              # D + T ->   + n
            'D-D_a': 'D_D_-_T_p.txt',            # D + D -> T + p
            'D-D_b': 'D_D_-_3He_n.txt',          # D + D -> 3He + n
            'D-3He': 'D_3He_-_4He_p-endf.txt',   # D + 3He ->   + p
            'p-B': 'p_11B_-_3a.txt',             # p + 11B -> 3
            #'p-p': 'p_p_-_B11.txt',
           }

xs = {}
for xs_id, xs_name in xs_names.items():
    xs[xs_id] = Xsec.read_xsec(xs_name)
# Total D + D fusion cross section is due to equal contributions from the
# above two processes.
```

```
xs['D-D'] = xs['D-D_a'] + xs['D-D_b']

def get_reactivity(xs, T):
    T = T[:, None]

    fac = 4 / np.sqrt(2 * np.pi * xs.mr * u)
    fac /= (1000 * T * e)**1.5
    fac *= (1000 * e)**2
    func = fac * xs.xs * Egrid * np.exp(-Egrid / T)
    I = np.trapz(func, Egrid, axis=1)
    # Convert from m3.s-1 to cm3.s-1
    return I * 1.e6

T = np.logspace(0, 3, 100)

xs_labels = {'D-T': '${D-T}$',
             'D-D': '${D-D}$',
             'D-3He': '${D-He^3}$',
             'p-B': '${p-B^{11}}$',
             #'p-p': '${p-p}$',
             }


fig = plt.figure(figsize=(8, 9), dpi=100)
ax = fig.add_subplot(111)

```

```
for xs_id, xs_label in xs_labels.items():
    ax.loglog(T, get_reactivity(xs[xs_id], T), label=xs_label, lw=2)

ax.legend(loc='upper left')

ax.grid(True, which='both', ls='-')
ax.set_xlim(1, 1000)
ax.set_ylim(1.e-20, 1.e-14)

xticks= np.array([1, 10, 100, 1000])
ax.set_xticks(xticks)
ax.set_xticklabels([str(x) for x in xticks])
ax.set_xlabel('$T$ (keV)')
ax.set_ylabel(r'$\langle \sigma v\rangle \; (\mathrm{cm^3\,s^{-1}})$')
plt.savefig('reactivity.png', dpi=300)
plt.show()

# Plot resolution (dpi) and figure size (pixels)
fig = plt.figure(figsize=(8, 6), dpi=100)
ax = fig.add_subplot(111)

for xs_id, xs_label in xs_labels.items():
    ax.loglog(Egrid, xs[xs_id], lw=2, label=xs_label)

ax.grid(True, which='both', ls='-')
ax.set_xlim(1, 1000)
```

```
xticks= np.array([1, 10, 100, 1000])
ax.set_xticks(xticks)
ax.set_xticklabels([str(x) for x in xticks])

if COFM:
    xlabel ='E (keV)'
else:
    xlabel ='E (keV)'
ax.set_xlabel(xlabel)

ax.set_ylabel('$\sigma\ ({m^2})$')
ax.set_ylim(1.e-32, 1.e-27)

ax.legend(loc='upper left')
plt.savefig('crosssections.png', dpi=300)
plt.show()

T_FDR = 300
reactivity_FDR = {}

for xs_id, xs_label in xs_labels.items():
    reactivity = get_reactivity(xs[xs_id], np.array([T_FDR]))
    # Compute for T=50 keV
    reactivity_FDR[xs_id] = reactivity[0]
    # Extract the single value from array
```

```
    print(f"{xs_id} Reactivity at T = {T_FDR} keV: {reactivity[0]:.3e} cm³/s")
```

Appendix B

Second Appendix

Propulsion system analysis for FDR, IEC, and AIM.

```python
import numpy as np
from numpy import pi
from matplotlib import rc
import matplotlib.pyplot as plt
import pandas as pd
from sympy import symbols, Eq, solve

# At T = 10 keV, ov in cm3/s
ov = [1.184e-18, # D-D
      2.226e-19, # D-He3
      1.137e-16, # D-T
      4.205e-22, # p-B11
       ]

ov11 = 1.184e-18

# The energy within the FRC separatrix at peak compression
```

```
v_L = 4.31*4e3  # m/s
M_L = 0.365*4.31  # kg
C_fus = 4.3e-8  # Fusion Constant
G_I = 10
E_L = (0.5*M_L*(v_L)**2)*10**(-3) # Liner Energy, kJ
E_in = E_L
G_F = np.sqrt(M_L)*(G_I)*(C_fus)*(E_L*10**(3))**(11/8)
E_fus = G_F * E_in

# Energy Transfer
eta = 1
phi_ion = 520.2/(6.941e-3) # 74945.97320270856 kJ/kg

E_out = E_fus
E_K = (eta*E_out - phi_ion*M_L)

# Specific Impulse
g0 = 9.81 #m/s2
I_sp = (np.sqrt(2*((E_out*10**3)/M_L))/g0) #s

# Mass Ratio
c = 299792 # km/s, Speed of Light

dV = 0.055 # Fraction of c
dV = dV*c
MR = np.exp(dV*(10**3)/(I_sp*g0))
```

```

# Print Input Results
print('\nCalculated Results')
print('Fusion Energy = ',E_fus, 'kJ',
     '\nLiner Energy = ', E_L, 'kJ',
     '\nLiner Mass = ', M_L, 'kg',
     '\nFusion Gain = ', G_F,
     '\nEnergy Input to the Fusion Reaction = ', E_in, 'kJ',
     '\nEnergy from the Fusion Reaction = ', E_out, 'kJ',
     '\nKinetic (Propulsive) Energy = ', E_K, 'kJ',
     '\nSpecific Impulse = ', I_sp, 'sec',
     '\nMass Ratio = ', MR,
        )

a_CAP = 1 # kg/kW
a_SEP = 3.9374*(G_F)**(-0.537) # kg/kW
M_PL = 500 # kg
dT = 50 # years
dT = dT*365*24*60*60 # convert to seconds

print('\nUser Inputs based on mission objectives')
print('Specific Mass (CAP) = ',a_CAP, 'kg/kW',
     '\nSpecific Mass (SEP) = ',a_SEP, 'kg/kW',
     '\nPayload Mass = ', M_PL, 'kg',
     '\nMission Time = ', dT, 'sec',
        )
```

```

# Solve system of equations for unknowns
M_I, M_F, M_S, M_P, freq, P_SEP = symbols('M_I M_F M_S M_P freq P_SEP')
Equations = [
    Eq(M_I / M_F, MR),
    Eq(M_PL + M_S, M_F),
    Eq(M_PL + M_S + M_P, M_I),
    Eq(M_L*freq*dT, M_P),
    Eq((E_in/a_CAP) + (P_SEP/a_SEP) + 0.1*M_PL, M_S),
    Eq(P_SEP/freq, E_in),
    ]

solution = solve(Equations)

print('\nSystem of Equation Results')
print('Initial Mass = ', solution[M_I], 'kg',
     '\nFinal Mass = ', solution[M_F], 'kg',
     '\nStructural Mass = ', solution[M_S], 'kg',
     '\nPropellant Mass = ', solution[M_P], 'kg',
     '\nFrequency of Operation = ', solution[freq], 's-1',
     '\nPower reqd to charge fusion caps = ', solution[P_SEP], 'kW',
        )

# Define the Reactants and Products
# Molecular Weights of Species
MM_D = 2.0141017778  # Deuterium (D)
```

```
MM_p = 1.0078250319  # proton (p)
MM_He3 = 3.0160293220  # Helium-3 (He3)
MM_T = 3.0160492813  # Tritium (T)
MM_B11 = 11.0093052  # Boron-11 (B11)
MM_He4 = 4.002603254  # Helium-4 (He4)
MM_n = 1.00866491  # neutron (n)

# Atomic Numbers
Z_D = 1  # Deuterium (D)
Z_p = 1  # proton (p)
Z_He3 = 2  # Helium-3 (He3)
Z_T = 1  # Tritium (T)
Z_B11 = 5  # Boron-11 (B11)
Z_He4 = 2  # Helium-4 (He4)

# Mass Numbers
MN_D = 2  # Deuterium (D)
MN_p = 1  # proton (p)
MN_He3 = 3  # Helium-3 (He3)
MN_T = 3  # Tritium (T)
MN_B11 = 11  # Boron-11 (B11)
MN_He4 = 4  # Helium-4 (He4)

M_Prop = solution[M_P] * 1000  # Mass of Propellant, g
# Define Plasma Container
th = (0.25/10) * 4.31 # Hoop thickness, cm
```

```
w_h = 5 * 4.31 # Hoop Width, cm
rho_L = 0.534 # Liner (Lithium) Density, g/cm3
r_L = (M_L * 1000)/(2*pi*w_h*th*rho_L) # Liner Radius, cm
r_p = r_L - th # Plasma Radius, cm
V_f = pi * w_h * r_p**2 # Fuel Volume, cm3


print('\nPlasma Container - Lithium')
print('Hoop Thickness = ', th, 'cm',
     '\nHoop Width = ', w_h, 'cm',
     '\nLiner Density = ', rho_L, 'g/cm3',
     '\nLiner Radius = ', r_L, 'cm',
     '\nInner (Plasma) Radius = ', r_p, 'cm',
     '\nFuel (Plasma) Volume = ', V_f, 'cm3',
       )

# Fuel Composition
Ti = [100, 70, 20, 300]  # Ion Temperature, keV
Te = [76, 56, 18, 138]  # Electron Temperature, keV
ov = [5.007e-17, 1.087e-16, 4.341e-16, 2.576e-16]  # Reactivity, cm3/s
ov11 = [1.184e-18, 1.184e-18, 1.184e-18, 3.361e-16]
# Species 1 Reactivity, cm3/s
n_0 = [1e18, 5e17, 5e17, 5e17]  # Particle Density, particles/cm3
y = [0.5, 0.5, 0.5, 1/6]  # Species 2 Fraction

rhoR = ((M_Prop)/V_f)*(r_p) # Areal Density, g/cm2
```

```
Phi_I = ((M_Prop)/V_f)*(w_h) # Specific Column Density, g/cm2
N_R0 = 6.023 * 10**(23) # Avogadros Number, atoms/mol
g0 = 9.81e2  # cm/s2

# Species 1 - Deuterium (D), Deuterium (D), Deuterium (D), proton (p)
M1 = [MM_D, MM_D, MM_D, MM_p]  # Molecular Weight, g/mol
Z1 = [Z_D, Z_D, Z_D, Z_p]  # Atomic Number

# Species 2 - Deuterium (D), Helium-3 (He3), Tritium (T), Boron-11 (B11)
M2 = [MM_D, MM_He3, MM_T, MM_B11]   # Molecular Weight, g/mol
Z2 = [Z_D, Z_He3, Z_T, Z_B11]  # Atomic Number

# Fusion Reactions
# D-D
E_DD =  0.5*(0.82) + 0.5*(4.04 + 14.67) + 0.5*(2.45) # D-D Product MeV
E_DDne = 0.5*(2.45)  # D-D Neutron Product MeV
eps_DD = ((MM_D + MM_D) - (0.5*(MM_He3 + MM_n) + 0.5*(MM_T + \
        MM_p)))/(0.5*(MM_He3 + MM_n) + 0.5*(MM_T + MM_p))
N_DDe = (1-y[0])*n_0[0]*(Z_D/MN_D) + (y[0])*n_0[0]*(Z_D/MN_D)
# Particle Concentration Electron, particle/cm3

# D-He3 / Aneutronic
E_DHe3 = 3.67 + 14.67  # D-He3 Product, MeV
E_DHe3ne = 0  # D-He3 Neutron Product, MeV
eps_DHe3 = ((MM_D + MM_He3) - (MM_He4 + MM_p))/(MM_He4 + MM_p)
N_DHe3e = (1-y[1])*n_0[1]*(Z_D/MN_D) + (y[1])*n_0[1]*(Z_He3/MN_He3)
```

```
# Particle Concentration Electron, particle/cm3

# D-T
E_DT = 3.52 + 14.06 # D-T Product, MeV
E_DTne = 14.06  # D-T Neutron Product, MeV
eps_DT = ((MM_D + MM_T) - (MM_He4 + MM_n))/(MM_He4 + MM_n)
N_DTe = (1-y[2])*n_0[2]*(Z_D/MN_D) + (y[2])*n_0[2]*(Z_T/MN_T)
# Particle Concentration Electron, particle/cm3

# p-B11 / Aneutronic
E_pp = 1.022  # p-p Product, MeV
E_pB = 8.68  # p-B11 Product, MeV
E_pBne = 0  # p-B11 Neutron Product, MeV
eps_pB = ((MM_p + MM_B11) - (3*MM_He4))/(3*MM_He4)
N_pBe = (1-y[3])*n_0[3]*(Z_p/MN_p) + (y[3])*n_0[3]*(Z_B11/MN_B11)
# Particle Concentration Electron, particle/cm3

# Equation Inputs:
E_11 = [E_DD, E_DD, E_DD, E_pp]
E_12 = [E_DD, E_DHe3, E_DT, E_pB]
E_ne = [E_DDne, E_DHe3ne, E_DTne, E_pBne]
N_e = [N_DDe, N_DHe3e, N_DTe, N_pBe]

# Reference 2
# Burnup Fraction
b = 0.155 # Assumed burn-up fraction 0.1-1.0
```

```python

# Fraction of fuel mass converted to energy
eps = [eps_DD, eps_DHe3, eps_DT, eps_pB]

c = 3e10  # Speed of Light, cm/s
n = 1  # Total Number of Stages
xj = 1/n  # Stage Fraction (1/1)
L_ly = 4.24  # Distance, ly
L = L_ly * 9.461e17 # Distance, cm

print('\nFuel Composition')
print('Areal Density = ', rhoR, 'g/cm2'
     '\nSpecific Column Density = ', Phi_I, 'g/cm2'
     '\nBurnup Fraction = ', b,
     '\nFrac. Fuel Mass > Energy = ', eps,
     '\n'
        )

t_c, md_ex, w, F, ga, al, P_ex, P_t, P_abs, a0, t_bj, u_n, xt, PT, CT, MT = \
        [], [], [], [], [], [], [], [], [], [], [], [], [], [], [], []

for M_1, M_2, eps_, ov_, E_ne_, E_12_, E_11_, N_e_, Z1_, Z2_, y_, n_0_, ov11_,
T_i, T_e in zip(M1, M2, eps, ov, E_ne, E_12, E_11, N_e, Z1, Z2, y, n_0, ov11,
Ti, Te):
        N1 = n_0_ * (1-y_)
        N2 = n_0_ * y_
```

```

        # Confinement Time, sec
        tc = (((N1 * M_1) + (N2 * M_2))*b)/((M_1 + M_2)*\
                (N1 * N2)*(ov_)*(1-(b*eps_)))

        # Thrust Calculation
        md_fb = ((M_1 + M_2) / N_R0) * (N1 * N2) * (ov_) * V_f
        # Rest Mass of Fuel Burned, g/sec
        md_f = md_fb / b  # Fuel Flow Rate, g/sec
        md_ex_ = md_f * (1 - (b*eps_)) # Rest Mass of Fuel Exhausted, g/sec
        # These 2 values are the same just the bottom one is simplified
        md_ex_ = (V_f/(tc * N_R0)) * ((N1*M_1) + (N2*M_2))

        w_ = c * ((eps_*b * (2 - (eps_*b)))**(0.5)) # Exhaust velocity, cm/s
        F_ = md_ex_ * w_  # Thrust, dynes, g-cm/s2

        g0 = 980
        I_sp__ = F_/(md_ex_* g0)
        print(I_sp__)

        # Fractional Power Carried by Neutrons (gamma)
        ga_ = (0.5 * (1-y_)**2 * (ov11_) * E_ne_) / ((y_ * (1-y_) * (ov_) *\
                (E_12_)) + (0.5 * (1-y_)**2 * (ov11_) * E_11_))

        # Fractional Energy Lost (alpha)
        al_br = (5.35e-31 * N_e_ * ((N1*(Z1_**2)) + (N2*(Z2_**2))) *\
```

```
                (T_e**(0.5))) / (2.93e-12 * N1 * N2 * (ov_))
        theta = ((8.5e-21 * (((y_+1) * (T_i * T_e)) + ((y_+1)**2 *\
                (T_e**2)))) * (1 + (T_e / 204))) / (y_ * (1-y_) * (ov_))
        al_cr = 1e-2 * theta
        al_ = al_br + al_cr

        # Fusion Exhaust Power
        P_ex_ = 1e-13 * F_ * (w_/2)  # MW

        # Total Power Output from Fusion Reactor
        P_t_ = P_ex_ / (1 - (ga_ + al_))  # MW

        # Power absorbed by engine walls
        P_abs_ = (ga_ + al_) / ( (1 - (ga_ + al_)) * P_ex_)

        a0_cm = F_/M_Prop  # cm/s2
        a0_g = a0_cm/g0  # Dimensionless (in g)

        # Burning Time, sec
        t_bj_ = ((1-(eps_*b)) * I_sp) / ((1 + xj) * a0_g)

        # Total Distance Traveled During Propulsion, cm
        u_n_ = c * ((MR**(2*n*w_/c)) - 1) / ((MR**(2*n*w_/c)) + 1)
        # Burnout Velocity, cm/s
        xt_ = (0 * t_bj_) + (((c**2) / (a0_g*g0)) * (((1 + ((a0_g**2 *\
                g0**2 * t_bj_**2)/(c**2)))**(0.5)) - 1))
```

```python

        if xt_ > L:
                PT_ = t_bj_ * L / xt_ * 3.18e-8
                CT_ = 0
        else:
                # Mission Profile
                PT_ = 3.18e-8 * n * t_bj_  # Propulsion Time, yrs
                CT_ = 3.18e-8 * (L - xt_) / u_n_  # Coast Time, yrs

        MT_ = CT_ + PT_  # Mission Time, yrs

        # Fix units for plots
        md_ex_k = md_ex_ * 1e-3  # MFR Exhaust, kg/s
        w_k = w_ * 1e-5  # Exhaust Velocity, km/s
        F_k = F_ * 1e-5  # Thrust, kg-m/s2
        a0_k = a0_cm * 1e-5  # Initial Acceleration, km/s2
        u_n_k = u_n_ * 1e-5  # Burnout Velocity, km/s
        xt_k = xt_ * 1e-5  # Total Prop. Dist., km

        # Return solutions for each rxn type
        t_c.append(tc), md_ex.append(md_ex_k), w.append(w_k), F.append(F_k)
        ga.append(ga_), al.append(al_), P_ex.append(P_ex_), P_t.append(P_t_)
        a0.append(a0_k), t_bj.append(t_bj_), u_n.append(u_n_k), xt.append(xt_k)
        PT.append(PT_), CT.append(CT_), MT.append(MT_), P_abs.append(P_abs_)


```

```
FinalData = {
        'Confinement Time (sec)': t_c,
        'Mass Flow Exhaust (kg/s)': md_ex,
        'Exhaust Velocity (km/s)': w,
        'Thrust (kg-m/s2)': F,
        'Frac. Pwr Neutrons': ga,
        'Frac. Energy Lost': al,
        'Exhaust Power (MW)': P_ex,
        'Total Power (MW)': P_t,
        'Excess Power (MW)': P_abs,
        'Initial Acceleration (km/s2)': a0,
        'Burning time (s)': t_bj,
        'Burnout Velocity (km/s)': u_n,
        'Arrival Distance, L (km)': L * 1e-5,
        'Prop. Distance (km)': xt,
        'Prop. Time (years)': PT,
        'Coast Time (years)': CT,
        'Mission Time (years)': MT,
        '': ' ',
}

datafinal = pd.DataFrame(FinalData)
datafinal.index = ['D-D', 'D-He3', 'D-T', 'p-B11']
print(datafinal.T)
```

```
# Ref - A General Crit of Inertial Electrostatic Confinement Fusion System
# D-D, D-He3, D-T, p-B11
Ti = [100e3, 70e3, 20e3, 300e3]  # Ion Temperature, eV
Te = [76e3, 56e3, 18e3, 138e3]  # Electron Temperature, eV
y2 = [0.5, 0.5, 0.5, 1/6]  # Species 2 Fraction
rc = [2.5, 2.5, 1.5, 3]  # Core Radius, cm
re = [125, 125, 75, 150]  # Edge Radius, cm
R = [250, 250, 150, 300]  # Radius, cm
ov = [5.007e-17, 1.087e-16, 4.341e-16, 2.576e-16]  # Reactivity, cm3/s
Q = [3.7e6, 18.3e6, 17.6e6, 8.7e6]  # Energy Released per Reaction, eV
n_ce = [1e18, 5e17, 5e17, 5e17]  # Particle Density, particles/cm3
N_cusp = 8
k_H = 2
eta_e = 0.99
eta_i = 0.99
mu_i = 2
me = 9.1093837e-28  # Electron mass, g
M_fus = 10e3  # Mass fusion system, g
M_PL = 500e3  # Mass Payload, g
BG = [7.0e4, 4.1e4, 2.2e4, 8.5e4]  # Magnetic Field Strength, Gauss
E_w = [300e3, 210e3, 60e3, 900e3]  # Energy loss well, eV

ni1, ni2, x, Pfus, V_f2, M_P2, MR2, tc2, md_ex2, w2, F2, P_ex2, I_sp2,
a0_g2, tbj2, un2, xt2, PT2, CT2, MT2, P_elc, P_elg, P_ilg = \
        [], [], [], [], [], [], [], [], [], [], [], [], [], [],
        [], [], [], [], [], [], [], [], []
```

```
for Ti_, Te_, y2_, R_, ov_, Q_, n_ce_, Z2_, M1_, M2_, eps_, rc_, E_w_, re_,
B_ in zip(Ti, Te, y2, R, ov, Q, n_ce, Z2, M1, M2, eps, rc, E_w, re, BG):
        # Fuel Composition
        ni1_ = n_ce_ * (1-y2_)
        ni2_ = n_ce_ * (y2_)
        x_ = ni1_/ni2_
        V_f_ = (4/3) * pi * (rc_**3)  # Fuel Volume, cm3

        # Total Fusion Power, W
        Pfus_ = 2.68e-18 * ov_ * Q_ * (x_/((x_ + Z2_)**2)) * (n_ce_**2) *\
                (rc_**3)

        # ---------
        # Losses, W
        if x_ >= Z2_:
                # Electron Cusp Losses
                P_elc_ = Pfus_ * 6.26e18 * N_cusp * (k_H**2) * (Z2_) *\
                        ((E_w_**(3/2))/((ov_ * Q_ * (n_ce_**2) * (rc_**3))))
                # Electron Grid Losses
                P_elg_ = Pfus_ * 1.78e8 * Z2_ * (1-eta_e) * ((R_/re_)**2) *\
                        ((E_w_**(3/2))/((ov_ * Q_ * n_ce_ * rc_)))
        else:
                # Electron Cusp Losses
                P_elc_ = Pfus_ * 1.56e18 * (N_cusp) * (k_H**2) *\
                        (((x_ + Z2_)**2)/(x_)) * ((E_w_**(3/2))/((ov_ *\
                        Q_ * (n_ce_**2) * (rc_**3))))
```

```
                # Electron Grid Losses
                P_elg_ = 1.19e-10 * (1-eta_e) * (R_**2) *\
                        (n_ce_ * ((rc_/re_)**2)) * (E_w_**(3/2))

        # Ion Grid Losses
        P_ilg_ = 2.79e-12 * (1-eta_i) * (R_**2) * (n_ce_ *\
                ((rc_/re_)**2)) * (E_w_**(3/2)) / np.sqrt(mu_i)
        # ---------

        # Confinement Time, sec
        tc__ = (((ni1_ * M1_) + (ni2_ * M2_))*b)/((M1_ + M2_)*\
                (ni1_ * ni2_)*(ov_)*(1-(b*eps_)))

        # Thrust Calculation
        md_fb_ = ((M1_ + M2_) / N_R0) * (ni1_ * ni2_) * (ov_) * V_f_
        # Rest Mass of Fuel Burned, g/sec
        md_f_ = md_fb_ / b  # Fuel Flow Rate, g/sec
        md_ex_ = md_f_ * (1 - (b*eps_)) # Rest Mass of Fuel Exhausted, g/sec
        # These 2 values are the same just the bottom one is simplified
        md_ex__ = (V_f_/(tc__ * N_R0)) * ((ni1_*M1_) + (ni2_*M2_))

        w__ = c * ((eps_*b * (2 - (eps_*b)))**(0.5)) # Exhaust velocity, cm/s
        F__ = md_ex__ * w__  # Thrust, dynes, g-cm/s2

        # Required Exhaust Power
        P_ex__ = 1e-13 * F__ * (w__/2)  # MW
```

```

        I_sp__ = F__/(md_ex__ * g0)
        dV = 0.055*c
        MR_ = np.exp(dV/(I_sp__*g0))
        M_P__ = (MR_ - 1) * (M_PL + (M_fus + (0.1*M_PL)))

        a0_cm_ = F__/M_P__  # cm/s2
        a0_g_ = a0_cm_/g0  # Dimensionless (in g)

        # Burning Time, sec
        t_bj__ = ((1-(eps_*b)) * I_sp__) / ((1 + xj) * a0_g_)

        # Total Distance Traveled During Propulsion, cm
        u_n__ = c * ((MR_**(2*n*w__/c)) - 1) / ((MR_**(2*n*w__/c)) + 1)
        # Burnout Velocity, cm/s
        xt__ = ((n-1) * u_n__ * t_bj__) + (((c**2) / (a0_g_*g0)) *\
                (((1 + ((a0_g_**2 * g0**2 * t_bj__**2)/(c**2)))**(0.5)) - 1))



        # Mission Profile
        if xt__ > L:
                PT__ = t_bj__ * L / xt__ * 3.18e-8
                CT__ = 0
        else:
                PT__ = 3.18e-8 * n * t_bj__  # Propulsion Time, yrs
                CT__ = 3.18e-8 * (L - xt__) / u_n__  # Coast Time, yrs
```

```
        MT__ = CT__ + PT__  # Mission Time, yrs

        # Fix units for plots
        md_ex_k = md_ex__ * 1e-3  # MFR Exhaust, kg/s
        w_k = w__ * 1e-5  # Exhaust Velocity, km/s
        F_k = F__ * 1e-5  # Thrust, kg-m/s2
        u_n_k = u_n__ * 1e-5  # Burnout Velocity, km/s
        xt_k2 = xt__ * 1e-5  # Total Prop. Dist., km
        a0_k_ = a0_cm_ * 1e-5  # Initial Acceleration, km/s2

        ni1.append(ni1_), ni2.append(ni2_), x.append(x_), Pfus.append(Pfus_),
        V_f2.append(V_f_), M_P2.append(M_P__), MR2.append(MR_),
        tc2.append(tc__), md_ex2.append(md_ex_k), w2.append(w_k),
        F2.append(F_k), P_ex2.append(P_ex__), I_sp2.append(I_sp__),
        a0_g2.append(a0_k_), tbj2.append(t_bj__), un2.append(u_n_k),
        xt2.append(xt_k2), PT2.append(PT__), CT2.append(CT__), MT2.append(MT__),
        P_elc.append(P_elc_), P_elg.append(P_elg_), P_ilg.append(P_ilg_)

FinalData2 = {
        'Mass Ratio': MR2,
        'Fuel Volume (cm3)': V_f2,
        'Fusion Power (W)': Pfus,
        'Power Electron Cusp Loss (W)': P_elc,
        'Power Electron Grid Loss (W)': P_elg,
        'Power Ion Grid Loss (W)': P_ilg,
        'Propellant Mass (g)': M_P2,
```

```
        'Confinement Time (sec)': tc2,
        'Mass Flow Exhaust (kg/s)': md_ex2,
        'Exhaust Velocity (km/s)': w2,
        'Thrust (kg-m/s2)': F2,
        'Exhaust Power (MW)': P_ex2,
        'Specific Impulse (sec)': I_sp2,
        'Initial Acceleration (km/s)': a0_g2,
        'Burning time (s)': tbj2,
        'Burnout Velocity (km/s)': un2,
        'Prop. Distance (km)': xt2,
        'Prop. Time (years)': PT2,
        'Coast Time (years)': CT2,
        'Mission Time (years)': MT2,
        '': ' ',

}

datafinal2 = pd.DataFrame(FinalData2)
datafinal2.index = ['D-D', 'D-He3', 'D-T', 'p-B11']
print(datafinal2.T)


# Ref - AIAA 1990 Antimatter Induced Fusion Rocket Propulsion
# D-D, D-He3, D-T, p-B11
Ti = [100, 100, 100, 100]  # Ion Temperature, keV
Te = [100, 100, 100, 100]  # Electron Temperature, keV
```

```
y2 = [0.5, 0.5, 0.5, 1/6]  # Species 2 Fraction
rc = [0.4, 0.4, 0.4, 0.4]  # Core Radius, cm
R = [0.8, 0.8, 0.8, 0.8]
ov = [5.007e-17, 1.729e-16, 8.433e-16, 4.267e-17]  # Reactivity, cm3/s
Q = [3.7e6, 18.3e6, 17.6e6, 8.7e6]  # Energy Released per Reaction, eV
n_ce = [6e17, 6e17, 6e17, 6e17]  # Particle Density, particles/cm3
I_sp = [6.7e3, 6.7e4, 6.1e4, 6.1e5]
eue = [0.84, 0.84, 0.69, 0.69]  # Energy Utilization Factor
fpg = [1e5, 1e5, 2.2e4, 2.2e4]  # Fusion Power Gain

ni1, ni2, x, Pjet, V_f2, M_P2, MR2, tc2, md_ex2, w2, F2, P_ex2, I_sp2,
a0_g2, tbj2, un2, xt2, MT3, Mi3, Mf3, Mst3, Ma3, Mp3, Mpt3, PT3= \
        [], [], [], [], [], [], [], [], [], [], [], [], [], [], [],
        [], [], [], [], [], [], [], [], [], []
for Ti_, Te_, y2_, R_, ov_, Q_, n_ce_, Z2_, M1_, M2_, eps_, rc_, E_w_, re_,
B_, I_sp__, fpg_, eue_ in zip(Ti, Te, y2, R, ov, Q, n_ce, Z2, M1, M2, eps,
rc, E_w, re, BG, I_sp, fpg, eue):
        # Fuel Composition
        ni1_ = n_ce_ * (1-y2_)
        ni2_ = n_ce_ * (y2_)
        x_ = ni1_/ni2_
        V_f_ = (4/3) * pi * (R_**3)  # Fuel Volume, cm3

        # Confinement Time, sec
        tc__ = (((ni1_ * M1_) + (ni2_ * M2_))*b)/((M1_ + M2_)*\
                (ni1_ * ni2_)*(ov_)*(1-(b*eps_)))
```

```

    # Thrust Calculation
    md_fb_ = ((M1_ + M2_) / N_R0) * (ni1_ * ni2_) * (ov_) * V_f_
    # Rest Mass of Fuel Burned, g/sec
    md_f_ = md_fb_ / b  # Fuel Flow Rate, g/sec
    md_ex_ = md_f_ * (1 - (b*eps_)) # Rest Mass of Fuel Exhausted, g/sec
    # These 2 values are the same just the bottom one is simplified
    md_ex__ = (V_f_/(tc__ * N_R0)) * ((ni1_*M1_) + (ni2_*M2_))

    #w__= I_sp__ * g0 # Exhaust velocity, cm/s
    w__ = c * ((eps_*b * (2 - (eps_*b)))**(0.5))
    F__ = md_ex__ * w__  # Thrust, dynes, g-cm/s2

    # Jet Power
    P_jet_ = 1e-13 * 0.5 * F__ * (w__)  # MW

    dV = 0.055*c
    MR_ = ((1 + (dV/c)) / (1 - (dV/c)))**(c/(2*w__))
    lam = 0.2
    M_PL = 5e5

    Mo = (1/(1 + lam - (lam*MR_)))*M_PL
    Mst = Mo - M_PL
    Mprop = Mst/lam

    # Dry Weight
```

```
        Wf = g0 * Mo

        # Temporary units change for alpha beta solver
        F_k = F__ * 1e-5
        Wfk = Wf * 1e-3
        g0k = 9.81
        Lk = L * 1e-2

        #  alpha and beta constants
        alp, bet = symbols('alp bet')
        Equations = [
                Eq(((g0k * (I_sp__**2))/(F_k/Wfk)) * (1/bet) *\
                        (((1/((alp)**(0.5)))-1)**2), Lk),
                Eq(((g0k * (I_sp__**2))/(F_k/Wfk)) *\
                        (((1/((bet)**(0.5)))-1)**2), Lk),
                ]
        solution3 = solve(Equations, (alp,bet))

        alpha = solution3[0][0]
        beta = solution3[0][1]

        # Lorentz-Fitzgerald Contraction Factor
        gam = 1 / np.sqrt(1 - (w__/c)**2)

        # Antimatter Mass
        ma_ = (1/(2*(1+fpg_))) * ((gam-1)/(gam + (eue_-1))) *\
```

```
                ((MR_ - 1)/(1 + lam - (MR_ * lam))) * M_PL

        # Total Propellant Mass, antimatter + fusion reactants
        M_P_t = ma_ + Mprop
        Mb = Mo + Mprop
        Mi = MR_ * Mo

        # Total Mission Time
        t_ab_ = (I_sp__/(F__/Wf)) * (1/beta) * ((1/(alpha)) - 1)

        a0_cm_ = F__/M_P_t  # cm/s2
        a0_g_ = a0_cm_/g0  # Dimensionless (in g)

        # Burning Time, sec
        t_bj__ = ((1-(eps_*b)) * I_sp__) / ((1 + xj) * a0_g_)

        # Total Distance Traveled During Propulsion, cm
        u_n__ = c * ((MR_**(2*n*w__/c)) - 1) / ((MR_**(2*n*w__/c)) + 1)
        # Burnout Velocity, cm/s
        xt__ = ((n-1) * u_n__ * t_bj__) + (((c**2) / (a0_g_*g0)) *\
                (((1 + ((a0_g_**2 * g0**2 * t_bj__**2)/(c**2)))**(0.5)) - 1))

        PT__ = 3.18e-8 * t_bj__

        MT__ = t_ab_ * 3.18e-8  # Mission Time, yrs

```

```
        # Fix units for plots
        md_ex_k = md_ex__ * 1e-3  # MFR Exhaust, kg/s
        w_k = w__ * 1e-5  # Exhaust Velocity, km/s
        F_k = F__ * 1e-5  # Thrust, kg-m/s2
        u_n_k = u_n__ * 1e-5  # Burnout Velocity, km/s
        xt_k2 = xt__ * 1e-5  # Total Prop. Dist., km
        a0_k3 = a0_cm_ * 1e-5

        ni1.append(ni1_), ni2.append(ni2_), x.append(x_),
        V_f2.append(V_f_), M_P2.append(M_P__), MR2.append(MR_),
        tc2.append(tc__), md_ex2.append(md_ex_k), w2.append(w_k),
        F2.append(F_k), Pjet.append(P_jet_), I_sp2.append(I_sp__),
        a0_g2.append(a0_k3), tbj2.append(t_bj__), un2.append(u_n_k),
        xt2.append(xt_k2), Mi3.append(Mi), Mf3.append(Mo),
        Mst3.append(Mst), Ma3.append(ma_), Mp3.append(Mprop),
        Mpt3.append(M_P_t), MT3.append(MT__), PT3.append(PT__)


FinalData3 = {
        'Fuel Volume (cm3)': V_f2,
        'Confinement Time (sec)': tc2,
        'Mass Flow Exhaust (kg/s)': md_ex2,
        'Exhaust Velocity (km/s)': w2,
        'Thrust (kg-m/s2)': F2,
        'Exhaust Power (MW)': Pjet,
        'Specific Impulse (sec)': I_sp2,
```

```
        'Initial Acceleration (km/s)': a0_g2,
        'Burning time (s)': tbj2,
        'Burnout Velocity (km/s)': un2,
        'Prop. Distance (km)': xt2,
        'Prop Time (years)': PT3,
        'Mission Time (years)': MT3,
        '': ' ',
        'Masses (g) ----------': '----------------',
        'Initial Mass': Mi3,
        'Final Mass': Mf3,
        'Structural Mass': Mst3,
        'Antimatter Mass': Ma3,
        'Fusion Prop Mass': Mp3,
        'Total Prop Mass': Mpt3,
        '': ' ',
}

datafinal3 = pd.DataFrame(FinalData3)
datafinal3.index = ['D-D', 'D-He3', 'D-T', 'p-B11']
df_TH = datafinal3.loc[datafinal3.index.isin(['D-He3', 'D-T'])]
print(df_TH.T)
```

Appendix C

Dust Impact

(Impact frequency and energy deposition of interstellar dust.)

```
import numpy as np
from numpy import pi
from matplotlib import rc
import matplotlib.pyplot as plt
import pandas as pd
from sympy import symbols, Eq, solve
from cycler import cycler
from matplotlib.ticker import MultipleLocator
from matplotlib.ticker import FixedLocator
from matplotlib.ticker import ScalarFormatter

linestyle_cycler = cycler('linestyle',['-','--',':'])
plt.rc('axes', prop_cycle=linestyle_cycler)

p = 2.57e-27  # Avg Particle Matter Density, g/cm3
m = 2e-12  # Mean Dust Particle Mass, g
L_ly = 4.24  # Distance, ly
```

```
L = L_ly * 9.461e17 # Distance, cm
rhoLi = 530  # Density Lithium, g/cm3
rhoAl = 2700  # Density Aluminum, g/cm3


n_0 = p/m  # Mean Dust Particle Density, particles/cm3
N_tot = n_0*L  # Number of Dust Impact Events/Area, particles/cm2

A_0 = list(range(100,50000,100))  # Cross Sectional Area, cm2

f, EkLi1, EkAl1, EkLi2, EkAl2, EkLi3, EkAl3 = [], [], [], [], [], [], []
for A0_ in A_0:
    # Impact Frequency, impacts/s
    f_ = N_tot*(A0_)/(56.5245864592250 * 365 * 24 * 60 * 60)
    f.append(f_)

    # Dust Energy Deposition (Kinetic Energy), J
    EkLi_1 = 0.5e-7 * pi * rhoLi * ((400e-7)**2) * 0.1 * (24004 * 1e-5)**2
    EkAl_1 = 0.5e-7 * pi * rhoAl * ((400e-7)**2) * 0.1 * (24004 * 1e-5)**2

    EkLi_2 = 0.5e-7 * pi * rhoLi * ((400e-7)**2) * 1 * (24004 * 1e-5)**2
    EkAl_2 = 0.5e-7 * pi * rhoAl * ((400e-7)**2) * 1 * (24004 * 1e-5)**2

    EkLi_3 = 0.5e-7 * pi * rhoLi * ((400e-7)**2) * 10 * (24004 * 1e-5)**2
    EkAl_3 = 0.5e-7 * pi * rhoAl * ((400e-7)**2) * 10 * (24004 * 1e-5)**2

```

```
    # Total Energy Deposition Throughout Mission, J
    EkLi_1 = EkLi_1 * N_tot * A0_
    EkAl_1 = EkAl_1 * N_tot * A0_

    EkLi_2 = EkLi_2 * N_tot * A0_
    EkAl_2 = EkAl_2 * N_tot * A0_

    EkLi_3 = EkLi_3 * N_tot * A0_
    EkAl_3 = EkAl_3 * N_tot * A0_

    EkLi1.append(EkLi_1), EkAl1.append(EkAl_1)
    EkLi2.append(EkLi_2), EkAl2.append(EkAl_2)
    EkLi3.append(EkLi_3), EkAl3.append(EkAl_3)


A_0 = list(range(1,500,1))


fig, ax_dist = plt.subplots()
ax_dist.set_xlim(1, 500)
ax_dist.plot(A_0, f)
ax_dist.grid(True, which='both', ls='-')
ax_dist.set_xlabel("Shielding Cross Sectional Area $(m^2)$")
ax_dist.set_ylabel("Impact Frequency (impact/s)")
#ax_dist.legend()

```

```
plt.tight_layout()
plt.show()

# Lithium
fig, ax_dist = plt.subplots()
#ax_dist.set_xlim(1, 500)
ax_dist.plot(A_0, EkLi1, label='0.1 cm')
ax_dist.plot(A_0, EkLi2, label='1 cm')
ax_dist.plot(A_0, EkLi3, label='10 cm')
ax_dist.grid(True, which='both', ls='-')
ax_dist.set_xlabel("Shielding Cross Sectional Area $(m^2)$")
ax_dist.set_ylabel("Total Energy Deposition (J)")
ax_dist.legend()

plt.tight_layout()
plt.show()

# Aluminum
fig, ax_dist = plt.subplots()
#ax_dist.set_xlim(1, 500)
ax_dist.plot(A_0, EkAl1, label='0.1 cm')
ax_dist.plot(A_0, EkAl2, label='1 cm')
ax_dist.plot(A_0, EkAl3, label='10 cm')
ax_dist.grid(True, which='both', ls='-')
ax_dist.set_xlabel("Shielding Cross Sectional Area $(m^2)$")
ax_dist.set_ylabel("Total Energy Deposition (J)")
```

```
ax_dist.legend()

# Use scientific notation for y-axis
formatter = ScalarFormatter()
formatter.set_scientific(True)
formatter.set_powerlimits((-5, -5))
ax_dist.yaxis.set_major_formatter(formatter)

plt.tight_layout()
plt.show()
```